

**MODELING AND INTERACTIVE DESIGN OF  
MULTILAYERED SPHERICAL INFRARED OPTICAL FILTERS  
USING MIE THEORY**

by

Nicholas J. Hudak

A thesis submitted to the Faculty of the University of Delaware in partial fulfillment of the requirements for the degree of Master of Science in Electrical and Computer Engineering

Spring 2017

© 2017 Nicholas J. Hudak  
All Rights Reserved

**MODELING AND INTERACTIVE DESIGN OF  
MULTILAYERED SPHERICAL INFRARED OPTICAL FILTERS  
USING MIE THEORY**

by

Nicholas J. Hudak

Approved: \_\_\_\_\_  
Mark S. Mirotznik, Ph.D.  
Professor in charge of thesis on behalf of the Advisory Committee

Approved: \_\_\_\_\_  
Kenneth E. Barner, Ph.D.  
Chair of the Department of Electrical and Computer Engineering

Approved: \_\_\_\_\_  
Babatunde A. Ogunnaike, Ph.D.  
Dean of the College of Engineering

Approved: \_\_\_\_\_  
Ann L. Ardis, Ph.D.  
Senior Vice Provost for Graduate and Professional Education

## **ACKNOWLEDGMENTS**

I would like to thank my advisor, Dr. Mark “Big Dog” Mirotznik, for his support and guidance over the course of my graduate career here at the University of Delaware. I would also like to thank the rest of the hardworking and extremely gifted peers in my research lab, especially: Benjamin Garrett, Austin Good, Zachary Larimore, Victoria Carey, and Paul Parsons. Working every day in an environment full of motivated and enthusiastic people has excited me to explore new topics and push myself to pursue more ambitious goals in my research.

I would like to dedicate my work to my parents: Mary Silvestri and James Hudak. They have worked so hard to help provide me with an opportunity to pursue my degree here at the University, and I am especially grateful for their unconditional love and support.

## TABLE OF CONTENTS

LIST OF TABLES .....	vi
LIST OF FIGURES .....	vii
ABSTRACT .....	ix
Chapter	
1 INTRODUCTION ON OPTICAL FILTERS AND MODELING PARTICLE AEROSOLS .....	1
1.1 Introduction .....	1
1.2 Introduction to Thin Film Optical Filters .....	2
1.3 Introduction to Modeling Aerosols .....	5
1.3.1 Basic Equations for Attenuation by Optical Filter Aerosols .....	6
2 PARTICLE DESIGN .....	9
2.1 Particle Geometry .....	9
2.2 Material Selection .....	11
2.3 Introduction to Mie Theory .....	13
2.4 Multilayered Sphere Extinction .....	18
3 CODING AND OPTIMIZATION OF MULTILAYERED SPHERICAL PARTICLES .....	26
3.1 Custom Mie Code .....	26
3.1.1 Optimal Spheres Function .....	26
3.1.2 Custom Mie Coefficient Solver .....	30
3.2 Graphical User Interface .....	33
3.2.1 Design Parameters .....	34
3.2.2 Simulation Setup .....	36
3.3 Optimization Code .....	38
3.3.1 Simulated Annealing .....	39
3.3.2 Pattern Search .....	41
4 RESULTS AND APPLICATIONS .....	43
4.1 Single Particle Simulation for MWIR Stop-Band Filters .....	43

4.2	Single Particle Simulation for SWIR Pass-Band Filter .....	47
4.3	Validation of Results .....	52
5	CONCLUSIONS AND FUTURE WORK.....	55
5.1	Conclusions .....	55
5.2	Future Work.....	56
	REFERENCES .....	58

## **LIST OF TABLES**

Table 2.1: Material properties of common materials used in the visible and infrared. 12

## LIST OF FIGURES

Figure 1.1: 5-layer thin film reflector based on a high-low index dielectric stack, adapted from [3].	4
Figure 1.2: Simple aerosolized particle cloud attenuation model, adapted from [4].	5
Figure 2-1: Conductive rod scattering with major dimension parallel to electric field.	10
Figure 2-2: Conductive rod scattering with major dimension perpendicular to electric field.	10
Figure 2-3: Extinction cross-section (top) and extinction efficiency (bottom) for a latex sphere with an index of $n_s = 1.59$ in air, $n_m = 1$ , figure borrowed from [9].	17
Figure 2-4: Multilayered thin film spherical particle scatterer.	19
Figure 2-5: Multilayered concentric sphere particle geometry, adapted from [10].	21
Figure 3-1: Calculation of extinction and scattering efficiencies from the “Optimal_spheres” function.	28
Figure 3-2: Excerpt of “Optimal_spheres” function assigning a function value for an optimal pass-band filter device.	29
Figure 3-3: MATLAB™ implementation of Wiscombe’s truncation number.	31
Figure 3-4: MATLAB™ adaptation of Wang’s recursive algorithms.	32
Figure 3-5: MATLAB™ adaptation of Wang’s recursive Han function (Equation 36).	33
Figure 3-6: Design parameter sub-section of the Multilayered Spherical Optical Filter GUI.	35
Figure 3-7: Simulation setup section of the Multilayered Spherical Optical Filter GUI.	36
Figure 3-8: MATLAB™ GUI for multilayered spherical optical filter code.	37
Figure 3-9: In progress view of simulated annealing optimization including best (top) and current (bottom) designs.	40

Figure 3-10: In progress view of the Pattern Search optimization including best (top) and current (bottom) designs. ....	42
Figure 4-1: Aluminum complex index of refraction plotted against wavelength in the mid-wave infrared [16]. ....	43
Figure 4-2: Initial user GUI input for high mass extinction aluminum hollow sphere design. ....	44
Figure 4-3: Results of simulated annealing and pattern search optimization processes for MWIR broad stop-band filter. ....	45
Figure 4-4: Resulting filter profile of optimized MWIR aluminum hollow-core stop-band filter. ....	45
Figure 4-5: Render of MWIR stop-band filter (20-nm thick aluminum hollow-shell). ....	47
Figure 4-6: Complex index of refraction for silicon and silicon dioxide for $\lambda = 1\text{-}12\mu\text{m}$ [16]. ....	48
Figure 4-7: Initial user GUI input for narrow pass-band filter design. ....	49
Figure 4-8: Results of simulated annealing and pattern search optimization processes for SWIR narrow pass-band filter. ....	50
Figure 4-9: Resulting filter profile of optimized SWIR Si/SiO <sub>2</sub> pass-band filter. ....	51
Figure 4-10: Render of optimized SWIR pass-band filter design. ....	51
Figure 4-11: Mass Extinction Coefficient results for Lumerical™(left) and custom Mie code (right) for a 2- $\mu\text{m}$ SiO <sub>2</sub> microsphere with 20nm Al shell in the SWIR. ....	52
Figure 4-12: Mass Extinction Coefficient results for Lumerical™ (right) and custom Mie code (left) for a 1.95- $\mu\text{m}$ radius 20nm thick Al hollow-sphere in the MWIR. ....	53
Figure 4-13: Mass Extinction Coefficient results for Lumerical™ (right) and custom Mie code (left) for a multilayered Si/SiO <sub>2</sub> spherical particle in the SWIR. ....	54

## ABSTRACT

The ability to manipulate the electromagnetic spectrum has long been an important factor in the field of photonics, however traditional optical filters are largely restricted to simple geometries due to practical limitations in fabrication. Recent developments in manufacturing technology has given engineers the ability to relax these restraints. A newly developed custom RF magnetron sputter deposition system located here at the University of Delaware has enabled the uniform coating of spherical micro particles. With this new fabrication technique, micro particles can be engineered to exhibit numerous application-based extinction profiles to produce highly effective optical filter aerosols, and so the need to simulate these new devices has become imperative.

A custom Mie code was developed to assist in the design and modeling of non-homogeneous spheres with highly absorbing shells. By using the principles of classical Mie theory together with the implementation of a recursive algorithm scheme when calculating the Mie series coefficients, it is now possible to simulate the extinction and scattering efficiency curves for these highly absorbing multilayered spherical optical filters in the visible and infrared spectrum. The generated efficiency curves can then be passed through an optimization scheme depending on the user's intent for particle design.

The first part of this thesis will be focused on introducing the core concepts of optical filters and aerosol modeling. Next, the Mie theory and recursive algorithm methods employed in the custom optimization software will be explored. The custom Mie code, optimization schemes, and user interface will be outlined. This thesis will focus on two major designs, a particle with a high mass extinction coefficient in the

mid-wave infrared, (MWIR,  $\lambda = 8-12\mu\text{m}$ ) and a particle exhibiting a narrow pass-band filtering effect inside the short-wave infrared spectrum (SWIR,  $\lambda = 1-3\mu\text{m}$ ). The remainder of this thesis will present numerical validations of my findings.

## Chapter 1

# INTRODUCTION ON OPTICAL FILTERS AND MODELING PARTICLE AEROSOLS

### 1.1 Introduction

While the idea of filtering the electromagnetic spectrum with a collection of aerosolized microspheres sounds like an idea ripped from a science fiction movie, the original concept started out much more modestly. Some of the first man-made “optical filters” were created by aerosolizing visibly opaque powders to create simple band-stop filters inside the visible spectrum. The earliest documented use of these crude optical filters occurred in 1622, where the Dutch shot barrels of damp gunpowder into the wind to shelter landing infantry from the enemy’s sight in the Dutch-Portuguese War [1]. Traditional optical filters are still in use today, however a new desire to not only extinguish incident radiation, but to create unique extinction profiles in the infrared frequency bands of radiation has been rapidly developing. Current optical filter technology extends this concept by producing devices capable of selectively transmitting, reflecting, or extinguishing light of different wavelengths [2]. The ability to create application based optical filters on a spherical micro particle would allow for several exciting new applications. The modeling and design work introduced in this thesis provides a robust method for engineering high efficiency optical filters through aerosolized micro particles. These aerosols can be used to create electro-optically switched mirrors, tunable notch filters, and remote chemical and biological sensors. Although more work is to be done to fully perfect the fabrication of multi-layered

spherical micro particles, the promise held by its unique resonant effects encourage further design and simulation to extend its possible applications.

## 1.2 Introduction to Thin Film Optical Filters

The field of photonics has always been energized by the promise of operating at or near the speed of light. While technology in the photonics field continues to grow, it produces an increasing amount of optics based communication and sensing techniques, therefore a need for better and more versatile optical filters has developed. Optical filters are designed to modify each component of the frequency or phase of incident light by promoting the absorption or interference of the reflected and transmitted signals. Thus by sequencing specific materials or films with varying indices of refraction in order to redirect or extinguish specific wavelengths of light, innovative optical devices can be created. While optical filters use many different approaches to achieve the modification of incoming signals, this thesis will focus on thin film optical filters. Thin film optics require an understanding of basic electromagnetic theory to understand how the light is interfering with itself inside the multilayered structure. The basic theory is best summed up by Macleod in his book, *Thin Film Optical Filters* [3], in which he begins by defining a series of basic equations. First, the reflectance of light at a boundary between two media is described by Equation (1), in which  $R$ , the reflectance at a boundary, is related to the square of the ratio of the difference of the indices of refraction at the boundary over their sum.

$$R = \left[ \frac{(1 - \frac{n_2}{n_1})}{(1 + \frac{n_2}{n_1})} \right]^2 = \left[ \frac{n_1 - n_2}{n_1 + n_2} \right]^2 \quad (1)$$

By examining a simple material with negligible absorption and purely real index of refraction, we can see that a reflection inside of a lower index material as compared to

the adjoining medium will result in a negative value, or a  $180^\circ$  phase shift. Conversely, the reflection occurring in the higher index medium will produce a positive resultant with no phase shift. If a complex index of refraction is taken into account in which a material has a non-negligible absorption coefficient (imaginary component), the phase shift and amplitude can result in various intermediate values, and can be solved through complex algebra. When incident light strikes a boundary, most often the energy is split into two components, a reflected and transmitted beam. When the reflections occur from multiple locations, the recombined energy can result in a difference or sum of the multiple reflected paths. If the reflected beams are separated by  $180^\circ$  in phase they subtract from each other, or “destructively” interfere, while in-phase energy will sum, or “constructively” interfere. These interference patterns can lead to interesting designs in optical filters.

A common design approach of optical filters is to stack an alternating pattern of high and low index films on top of a substrate or device. The reflections caused at each boundary inside of the higher index films receive no phase shift, while the reflections inside the lower index material will be  $180^\circ$  out of phase, this provide designers with the ability to choose a specific film thicknesses and indices to encourage constructive or deconstructive interference when reflected signals overlap with the incident beam. One common example of this design is a single layer anti-reflection coating, which uses a single dielectric layer to cancel the reflected energy from an abrupt change in index. For complete cancellation in a single layer anti-reflective coating, the amplitude of the reflected energy must be equal at the upper and lower surfaces of the film, therefore the index of the layer must be equal to the square of the index of the surrounding medium and substrate as depicted in Equation (2).

$$\frac{n_0}{n_1} = \frac{n_1}{n_{sub}} \rightarrow n_1 = \sqrt{n_0 n_{sub}} \quad (2)$$

Additionally, the optical thickness of each layer is made to be a quarter wavelength of the incident light inside of the medium. This will ensure that the two reflections at the top and bottom surfaces of the layer will destructively interfere as they travel back towards the source of the incident light. This complete cancellation eliminates reflection and can be expanded upon by increasing the number of layers and broadening the bandwidth of the filter. Another application of high and low index alternating stacks is a high reflectivity film. If all films are kept at equal quarter wavelength thicknesses while alternating between a high and low index, the alternating phase shifted reflections will recombine constructively generating a reflectance proportional to the number of layers in the stack. Figure 1.1, adapted from *Thin Film Optical Filters* [3], depicts the cross-section of an alternating high-low index thin film reflector.

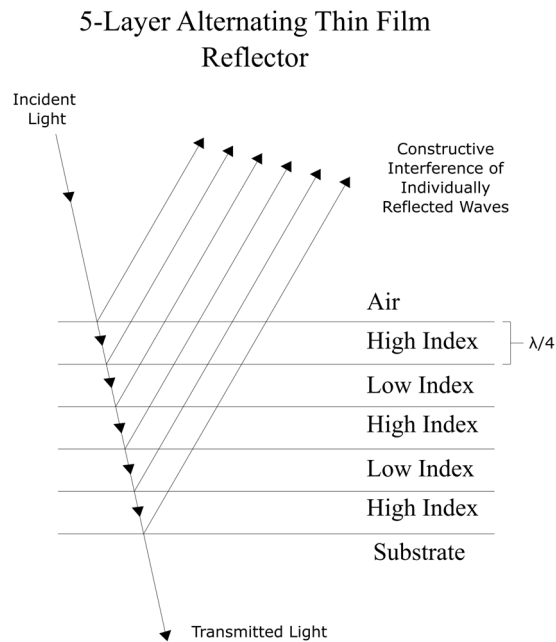


Figure 1.1: 5-layer thin film reflector based on a high-low index dielectric stack, adapted from [3].

### 1.3 Introduction to Modeling Aerosols

Aerosolized particles, as depicted below in Figure 1.2, are formed by dispersing a low transmission, superfine material into a medium, thus providing a barrier between the source of incident radiation and its intended target [4,5]. The aerosol's constituent particles work together to attenuate any penetrating electromagnetic energy either by scattering or absorption mechanisms. While both of these mechanisms are effective ways of extinguishing unwanted radiation, the particle's size, geometry, and material properties will determine how much of each contributes to the overall extinction of the energy at a specified wavelength. Given the specific application requirements, the particle size, material, and geometry must be carefully selected as the contribution of each individual particle will shape the overall characteristics of the aerosol.

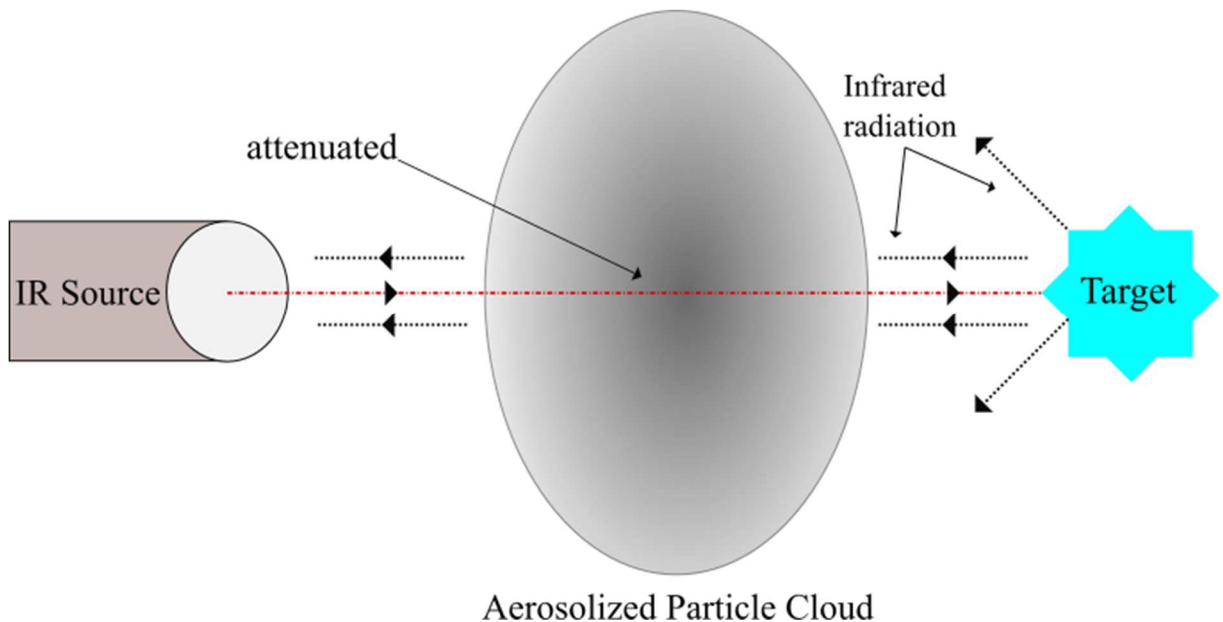


Figure 1.2: Simple aerosolized particle cloud attenuation model, adapted from [4].

### 1.3.1 Basic Equations for Attenuation by Optical Filter Aerosols

Considering the situation depicted in Figure 1.2, the incoming energy emitted from the infrared source will be attenuated as a function of distance travelled through the aerosol. The series of equations we will define in the upcoming section have been described by Shi, in their article, “Infrared extinction of artificial aerosols and the effects of size distributions” [4]. The further the beam must travel through the aerosol to reach the target, the more heavily attenuated the beam will become. Therefore, the transmitted irradiance can be calculated by Equation (1).

$$I_t = I_0 e^{-\int_0^L \beta(\lambda) dx} \quad (3)$$

where  $I_0$  is the incident irradiance,  $L$  is thickness of the aerosolized cloud,  $\lambda$  is the wavelength of the incident irradiation, and  $\beta(\lambda)$  is the extinction coefficient at a particular wavelength. An extinction coefficient quantifies the aerosol’s ability to attenuate incident energy of a certain wavelength. It is a function of both the number density of particulates,  $N$ , and the extinction cross-section of each individual particle,  $\sigma_E$ .

$$\beta(\lambda) = N\sigma_E(\lambda) \quad (4)$$

Equations (3) and (4) can be adapted to incorporate the likely condition that a relative size distribution exists within the constituent micro particles. If we were to have an aerosol of micro particles ranging from 1-3 $\mu\text{m}$  in diameter we would want to represent that variety by representing  $\sigma_E$  as a function of both particle diameter,  $D$ , as well as wavelength,  $\lambda$ . Additionally, a distribution of the varying particle diameters would be represented by the function  $f(D)$ . With these changes, the extinction coefficient would now be best described by Equation (5).

$$\beta(\lambda) = \int_0^\infty N\sigma_E(\lambda, D)f(D)dD \quad (5)$$

Since we will most likely be observing the aerosol's performance within a given wavelength band, (SWIR/MWIR), it is normally advantageous to represent the extinction coefficient as an average across the band of interest. In this case a standard averaging equation will be modified to calculate  $\bar{\beta}$ , the average extinction coefficient across a the band.

$$\bar{\beta} = \frac{1}{\lambda_2 - \lambda_1} \int_{\lambda_1}^{\lambda_2} \beta(\lambda) d\lambda \quad (6)$$

It is important to remember that while it may be trivial to design a particle with a high extinction coefficient, it is equally important to examine the particle's mass, as its total weight will ultimately determine the time duration that the aerosol can remain suspended within its respective medium. We can examine the extinction capability of a material per unit mass by using the following expression,

$$\beta_m(\lambda) = \frac{\beta(\lambda)}{M} \quad (7)$$

where  $\beta_m$  is known as the mass extinction coefficient, and M represents the total mass of N particles. We can solve for the mass by integrating the total volume of each subset of micro particle diameters and multiplying by the mass density of each (This equation will be adjusted based on the geometry of the constituent particles inside of the aerosol).

$$M = \int_0^{\infty} N f(D) \frac{1}{6} \pi D^3 \rho dD \quad (8)$$

If we examine Equations (5), (7), and (8) we can obtain a general expression that shows in order to attain a mass extinction coefficient for a particular aerosol we must first obtain the extinction cross-section of each particle,  $\sigma_e$ , as well as the distribution function of the particle sizes inside the aerosol,  $f(D)$ .

$$\beta_m(\lambda) = \frac{6 \int_0^{\infty} \sigma_E(\lambda, D) f(D) dD}{\pi \rho \int_0^{\infty} D^3 f(D) dD} \quad (9)$$

By using Equation (7) together with the averaging seen in Equation (6) we can produce our most comprehensive and final equation to describe the average mass extinction coefficient of the given aerosol over a set band of wavelengths.

$$\bar{\beta}_m = \frac{1}{\lambda_2 - \lambda_1} \int_{\lambda_1}^{\lambda_2} \beta_m(\lambda) d\lambda \quad (10)$$

Now that we have covered the basics of thin film optical filters, and outlined a way to quantify the efficiency of both the individual particles and overall aerosol based upon the extinction cross-section of a single particle, we will turn our attention to the specific design of multilayered particles. Specifically, we will need to discuss how the particle geometry and material properties will be used to determine an effective extinction cross-section.

## Chapter 2

### PARTICLE DESIGN

#### 2.1 Particle Geometry

Many different geometries were explored when determining an ideal micro particle for simulation. High aspect ratio metallic particles such as flakes and rods were first explored due to their connection with known surface plasmon resonant (SPR) effects, which are capable of producing high mass extinction coefficients [6]. However, these high mass extinction coefficients were found to be both highly dependent upon the orientation of the particle in respect to the polarization of the incident light, and narrow-band in the IR. This orientation dependency can be best described by examining the effects of polarization in the incident energy. If high aspect ratio particles were to be used in my design, the scattered energy would peak when the polarization of the incident E-field was aligned parallel to the major dimension of the particle, thus any random motion or disorder would cause a decrease in extinction from the ideal case of complete parallel alignment of each particle in the aerosol. This scattering peak is caused by the formation of surface currents on the conductive surface opposing the incident electric field [7]. If the field is aligned parallel to the major axis, the largest path for the surface current to propagate would be seen, thus re-radiating or “scattering”, the highest possible percentage of incident energy. If this orientation is changed, the path length of the generated surface currents would decrease as would its scattering effects. This phenomenon is best illustrated in Figures 2-1 and 2-2.

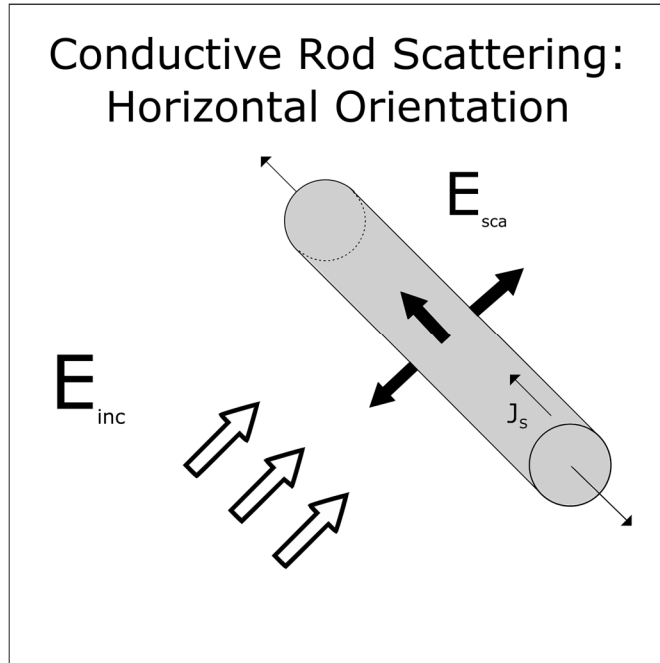


Figure 2-1: Conductive rod scattering with major dimension parallel to electric field

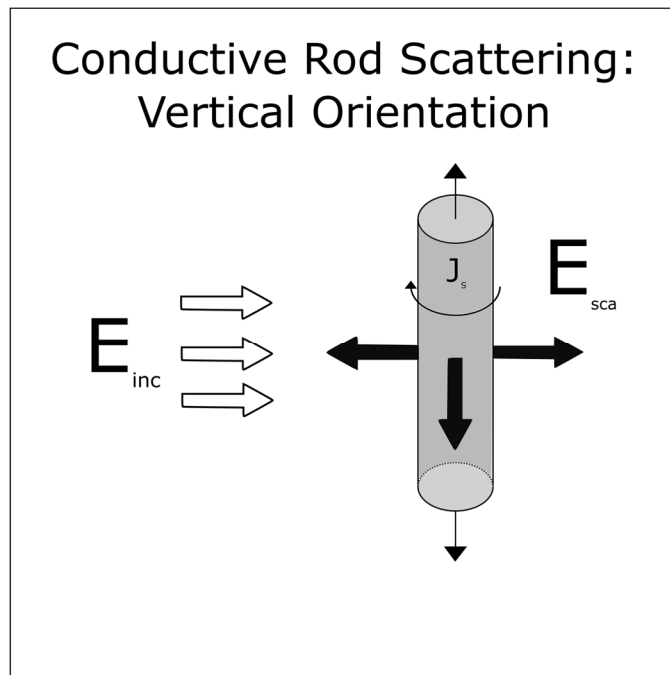


Figure 2-2: Conductive rod scattering with major dimension perpendicular to electric field

To get around this challenge, a spherical geometry was chosen to ensure spatial symmetry and eliminate a variation in scattering due to particle orientation or the polarization of the incident energy.

By focusing on a traditional spherical geometry, Mie Theory can more easily be used to determine the specific extinction behavior of an individual particle. Mie Theory will lay the groundwork for the custom Mie software that will be introduced in Chapter 3.

## **2.2 Material Selection**

When considering the materials that will contribute to a particular optical filter design it is important to have an understanding of their performance and characteristics in the frequency spectrum of intended use. Material properties typically change over frequency (dispersion), and because of that popular material choices for visible wavelength optical filters may not be the best choice for a filter designed in the infrared. The material's transparency, density, abbe number, index of refraction, and absorption will all need to be carefully examined and assessed for each specific application. It is also important to consider the conditions that the device will be exposed to, the required mechanical strength of a device, and ease of fabrication need to be considered when making an informed decision. The devices discussed in this thesis may be deployed in a variety of situations, so the specific material decisions will be detailed later in the application specific section of this thesis.

The most frequently used materials for filter design in the visible and infrared spectrum are shown below in Table 2.1 [8].

Table 2.1: Material properties of common materials used in the visible and infrared.

<b>Material</b>	<b>Index of Refraction (n)</b>	<b>Density (g/cm<sup>3</sup>)</b>	<b>Abbe Number (v<sub>d</sub>)</b>
Polystyrene (C <sub>8</sub> H <sub>8</sub> ) <sub>n</sub>	1.570	1.04	29.53
Calcium Fluoride (CaF <sub>2</sub> )	1.434	3.18	95.1
Silicon Dioxide (SiO <sub>2</sub> )	1.456	2.65	67.8
Germanium (Ge)	4.003	5.33	N/A
Magnesium Fluoride (MgF <sub>2</sub> )	1.413	3.18	106.2
N-BK7	1.517	2.46	64.2
Potassium Bromide (KBr)	1.527	2.75	33.6
Sapphire (Al <sub>2</sub> O <sub>3</sub> )	1.768	3.97	72.2
Silicon (Si)	3.422	2.33	N/A
Sodium Chloride (NaCl)	1.491	2.17	42.9
Zinc Selenide (ZnSe)	2.403	5.27	N/A
Zin Sulfide (ZnS)	2.4631	5.27	N/A
Aluminum (Al)	.6332-32.109	2.70	N/A
Titanium Dioxide (TiO <sub>2</sub> )	2.4538	1.71	9.87

As expressed earlier, two major design focuses in this thesis are to create a narrow pass-band filter in the SWIR and a broad stop-band filter in the MWIR. The

three primary materials we will be using to complete our design are silicon, silicon dioxide, and aluminum, although all of the materials listed in Table 2.1 could be used for various filtering applications.

### **2.3 Introduction to Mie Theory**

After selecting a spherical particle base geometry, we can now turn our attention toward obtaining the scattering cross-section of an individual particle. First it is important to understand the physics behind the attenuation of incident radiation when interacting with matter. The equations and basic principles found in this section are well summarized by Ng [9]. All matter is made up from small electrical charges known as electrons and protons. These charges are set into an oscillatory motion when excited by incident radiation. This oscillation in turn leads to a re-radiation of energy known as scattering. Another mechanism in which materials can attenuate incident radiation is through absorption, in which incident energy upon a material is extinguished rather than re-radiated. Absorption occurs in materials with a complex index of refraction,  $m$ , as shown in Equation (11) the real part of the index determines the material's index of refraction,  $n$ , while the imaginary part,  $k$ , contributes to absorption and is known as the attenuation coefficient.

$$m = n + ik \quad (11)$$

The total amount of radiation that is extinguished in an incident beam when travelling through a material is known as extinction, and it incorporates both scattering and absorption losses. Two of the possible theories to consider when describing the interaction of incident radiation with a spherical particle are Mie theory and ray optics. Mie theory is based upon Maxwell's equations in which the incident, scattered, and internal fields are derived. The expressions of the fields take the form of an infinite

series of vector spherical harmonics (VSWF). With these expressions it is possible to find cross-sections, efficiency factors, and intensity distributions on a homogeneous particle. One aspect of Mie theory we will focus on is morphology dependent resonance (MDR), where the particle resonances are generated by varying a size parameter,  $\chi$ . The size parameter is a function of the particle radius,  $a$ , and the wavelength of incident radiation in the surrounding medium,  $\frac{\lambda_0}{n_m}$ , as seen in Equation (12).

$$\chi = \frac{2\pi a n_m}{\lambda_0} \quad (12)$$

The micro particles we aim to design must be light enough to remain suspended in air, therefore we are practically limited to particle diameters less than 30 $\mu$ m depending on particle density. At this particle size, the diameter of the particle will be comparable to the wavelength of the incident light in which case Mie theory becomes the preferred tool to examine the particle's extinction cross-section.

For the rest of this introduction to Mie Theory, we will focus on the general case in which a plane wave excitation is incident upon a homogeneous spherical particle. The electric field is polarized in the x direction and travels in the z direction with an amplitude of  $E_0$  and propagation constant of  $\beta_0$ . As seen in Equation (13).

$$\vec{E}_{inc} = E_0 e^{-i\beta_0 z} \hat{x} \quad (13)$$

We can use Maxwell's equations to solve for the time dependent vector wave equations in Equations (14a) and (14b)

$$\nabla^2 \vec{E} + k_m^2 \vec{E} = 0 \quad (14a)$$

$$\nabla^2 \vec{H} + k_m^2 \vec{H} = 0 \quad (14b)$$

Where  $k_m^2 = \omega^2 \epsilon_m \mu$  represents the wave vector in the surrounding medium and  $\epsilon_m$  is the permittivity in that medium. Now, we need to derive the vector solutions of the wave

equation by applying a spherical coordinate system centered around the base particle geometry, defining a scalar function  $\psi_{l,m}$ , and a constant vector  $\vec{r}$ . If the scalar function is a solution of the wave equation, we can find two independent vector solutions,  $\vec{M}_{l,m}$  and  $\vec{N}_{l,m}$  which are solenoidal of each other much like  $\vec{E}$  and  $\vec{H}$  as shown in Equations (15a) and (15b).

$$\vec{M}_{l,m} = \nabla \times \vec{r} \psi_{l,m} \quad (15a)$$

$$\vec{N}_{l,m} = \frac{1}{k_m} \nabla \times \vec{M}_{l,m} \quad (15b)$$

These vector spherical harmonics can be used to express the internal and scattered electric and magnetic fields, which are shown in the set of equations

$$\vec{E}_{sca} = \frac{k_m}{\omega^2 \epsilon_m \mu} \sum [A_{l,m} a_l \vec{M}_{l,m} + B_{l,m} b_l \vec{N}_{l,m}] \quad (16a)$$

$$\vec{H}_{sca} = -\frac{ik_m}{\omega \mu} \sum [A_{l,m} a_l \vec{N}_{l,m} + B_{l,m} b_l \vec{M}_{l,m}] \quad (16b)$$

$$\vec{E}_{int} = \frac{k_m}{\omega^2 \epsilon_m \mu} \sum [A_{l,m} c_l \vec{M}_{l,m} + B_{l,m} d_l \vec{N}_{l,m}] \quad (16c)$$

$$\vec{H}_{int} = -\frac{ik_m}{\omega \mu} \sum [A_{l,m} c_l \vec{N}_{l,m} + B_{l,m} d_l \vec{M}_{l,m}] \quad (16d)$$

$A_{l,m}$  and  $B_{l,m}$  represent expansion coefficients characteristic of a specific incident beam of energy,  $a_l$  and  $b_l$  are scattering coefficients, and  $c_l$  and  $d_l$  are coefficients of the internal fields, which can be determined from the boundary conditions located at the surface of the sphere.

$$[\vec{E}_{inc} + \vec{E}_{sca} - \vec{E}_{int}] \times \vec{r} = 0 \quad (17a)$$

$$[\vec{H}_{inc} + \vec{H}_{sca} - \vec{H}_{int}] \times \vec{r} = 0 \quad (17b)$$

By using the boundary conditions together with the definitions for the fields provided above, the Mie coefficients ( $a_l$ ,  $b_l$ ,  $c_l$ , and  $d_l$ ) can be calculated.

With these coefficients and the intensity incident on the particle we can calculate the scattered and extinction energies, and furthermore the scattering, extinction, and absorption cross-sections.

$$\sigma_{sca} = \frac{2\pi}{k_m^2} \sum_{l=1}^{\infty} (2l+1) (|a_l|^2 + |b_l|^2) \quad (18a)$$

$$\sigma_{ext} = \frac{2\pi}{k_m^2} \sum_{l=1}^{\infty} (2l+1) (a_l + b_l) \quad (18b)$$

$$\sigma_{abs} = \sigma_{ext} - \sigma_{sca} \quad (18c)$$

From the extinction cross-section, an extinction efficiency can be calculated by dividing by the geometrical cross-section of your particle.

$$Q_{sca} = \frac{\sigma_{sca}}{\pi r^2} \quad (19a)$$

$$Q_{ext} = \frac{\sigma_{ext}}{\pi r^2} \quad (19b)$$

Finally, a mass-extinction coefficient ( $m^2/g$ ) can be found by dividing the extinction efficiency by the mass of the particle.

$$\text{mass extinction coefficient} = \alpha = \frac{Q_{ext}}{m_p} \quad (20a)$$

When the scattering or extinction efficiency of a spherical particle is plotted vs the size parameter,  $\chi$ , it is evident that there exists an extinction efficiency peak at a particular size parameter given the index of the surrounding medium and of the scattering sphere. Figure 2-3 compares the plots of both the extinction efficiency and extinction cross-section of a homogeneous latex sphere with  $n_s = 1.59$ ,  $n_m = 1$ , against the size parameter of the sphere with  $\lambda = 1\mu m$ .

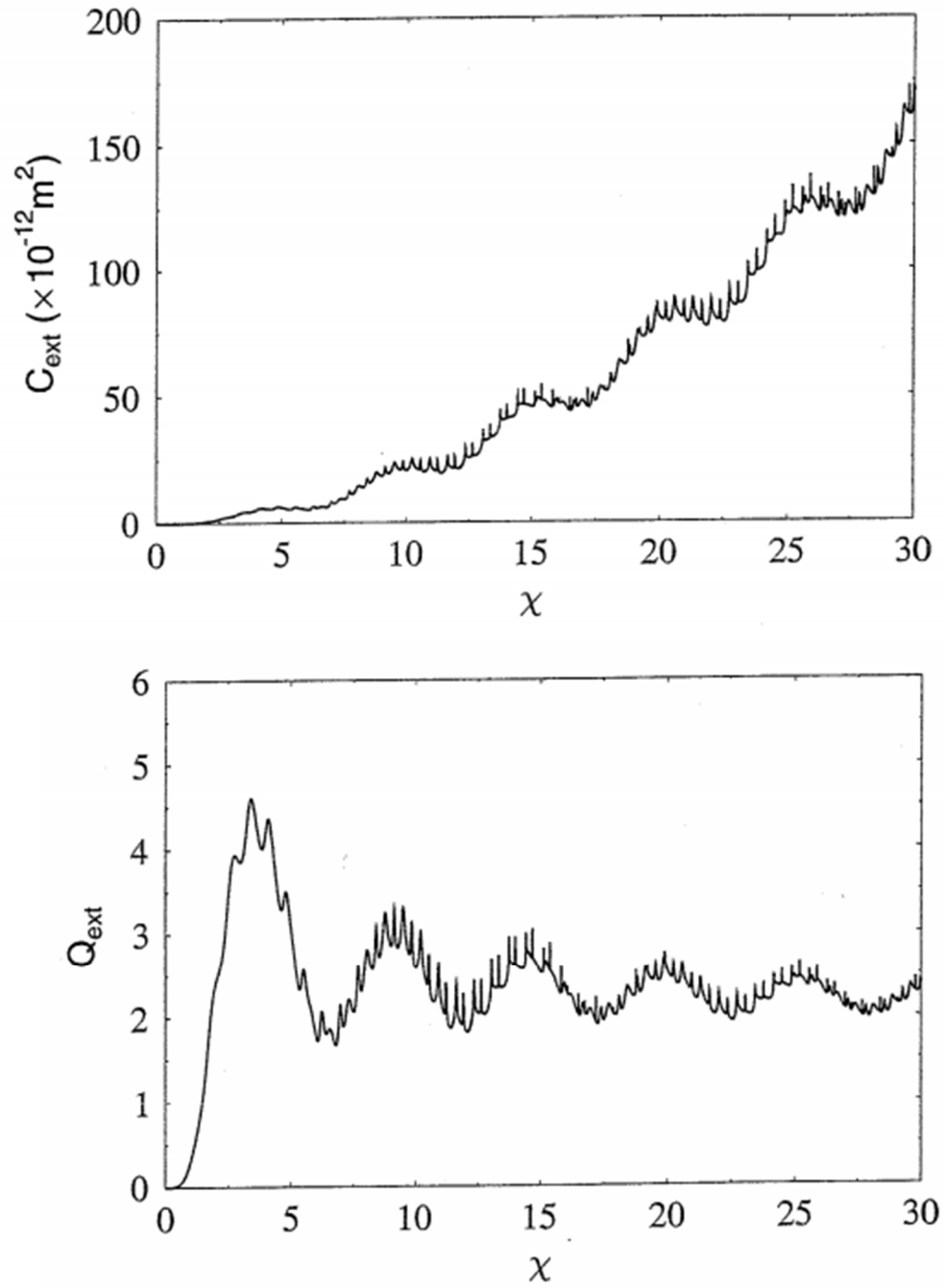


Figure 2-3: Extinction cross-section (top) and extinction efficiency (bottom) for a latex sphere with an index of  $n_s = 1.59$  in air,  $n_m = 1$ , figure borrowed from [9].

In the figure it is easily seen that while the scattering cross-section continues to rise as the size parameter of the sphere grows, the efficiency of the scattering relative to the size of your particle has a series of resonances, which reach a maximum peak when the radius of the particle is roughly equal to the wavelength of the incident light. This efficiency peak will come in handy when designing particles in the short and mid infrared frequency bands for optimal extinction.

## **2.4 Multilayered Sphere Extinction**

While the classical Mie theory explained above is well suited for describing the extinction characteristics of a homogeneous sphere, the theory must be adapted to take advantage of the multilayered design proposed in this thesis. The idea behind the basic geometry of a multilayered spherical scatterer is to explore the effect of layered dielectric and metallic films when surrounding a spherical core substrate in order to reproduce filter profiles seen in traditional planar structures. If the thin film interference described in Section 1.2 could be replicated in a spatially symmetric shape, the dependence on the angle of incidence for incoming signals could be avoided, therefore producing a much more robust optical filter that could maintain function while experiencing the random motion frequently exhibited by aerosols. The basic alternating high and low index layered sphere design is shown in Figure 2-4.

This design will be the basis for the simulations presented in Chapter 4. The boundary conditions at each interface will need to be solved starting from the inside of the sphere and continuing outwards, until the final scattering coefficients can be extracted in order to characterize the sphere at the outermost surface, generalizing the functionality of the particle as a whole. The recursive algorithm approach we will take in our optimization software for obtaining these Mie series coefficients is outlined in

Wen Yang's journal article titled, "Improved Recursive Algorithm for Light Scattering by a Multilayered Sphere" [10], I recommend reading this article to receive further background on the functions and variables pertaining to Yang's algorithm that will be outlined in the rest of this section.

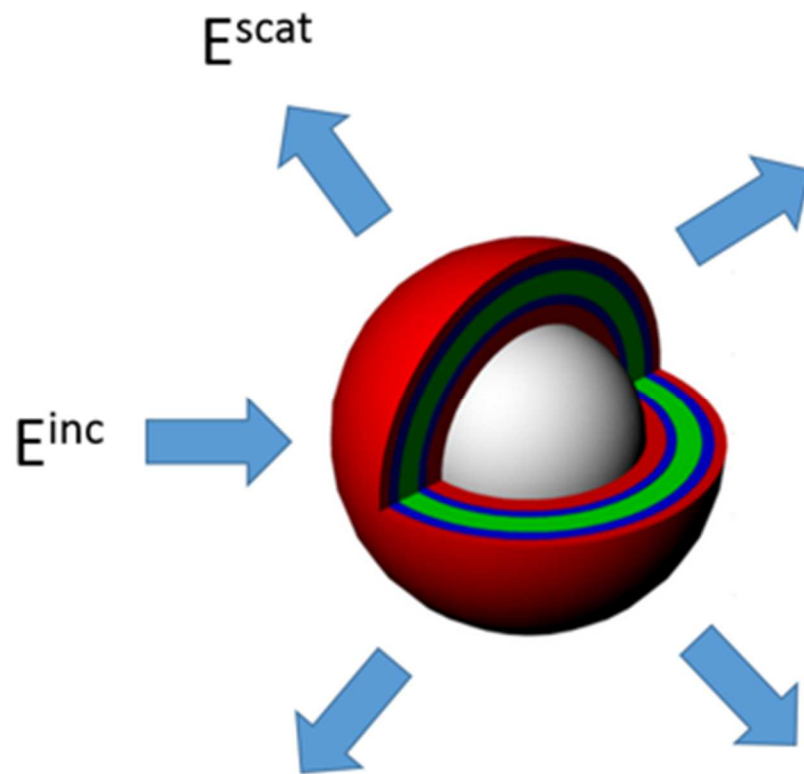


Figure 2-4: Multilayered thin film spherical particle scatterer

A great number of contributing authors have adapted and improved upon the original model of EM scattering from a sphere first worked out by Aden and Kerker [11], with a number of recent iterations attempting to include thin shelled and non-

homogeneous spherical particles in their calculations [12-15]. An abundance of these types of spherical particles are found in nature, and the need to model the scattering behavior of finely stratified or large and heavily absorbing particles has until very recently endured numerical errors caused by round-off and overflow problems originating from calculations of the Riccati-Bessel functions with large complex arguments. In Yang's paper an improved recursive algorithm leveraging the calculation of the logarithmic derivatives of the Riccati-Bessel functions to recursively solve for the scattering coefficients,  $a_n$  and  $b_n$  has proven to increase numerical stability when considering particles with large size parameters, thin heavily absorbing shells, and finely stratified layers. It suggests that if we approach an iterative solving technique for a series of concentric spheres with varying size parameters rather than the discrete layer indicative of our design, we can rewrite our definitions for the size parameter and relative refractive index as

$$x_l = \frac{2\pi N r_l}{\lambda} = k r_l \quad (21a)$$

$$m_l = N_l / N = n_l + i k_l \quad (21b)$$

where  $N$ , is the index of refraction of the outside medium,  $N_l$  is the index inside the  $l^{\text{th}}$  layer of the sphere,  $\lambda$  is the wavelength of the incident wave,  $r_l$  is the radius of the  $l^{\text{th}}$  layer, and  $k$  is the propagation constant.

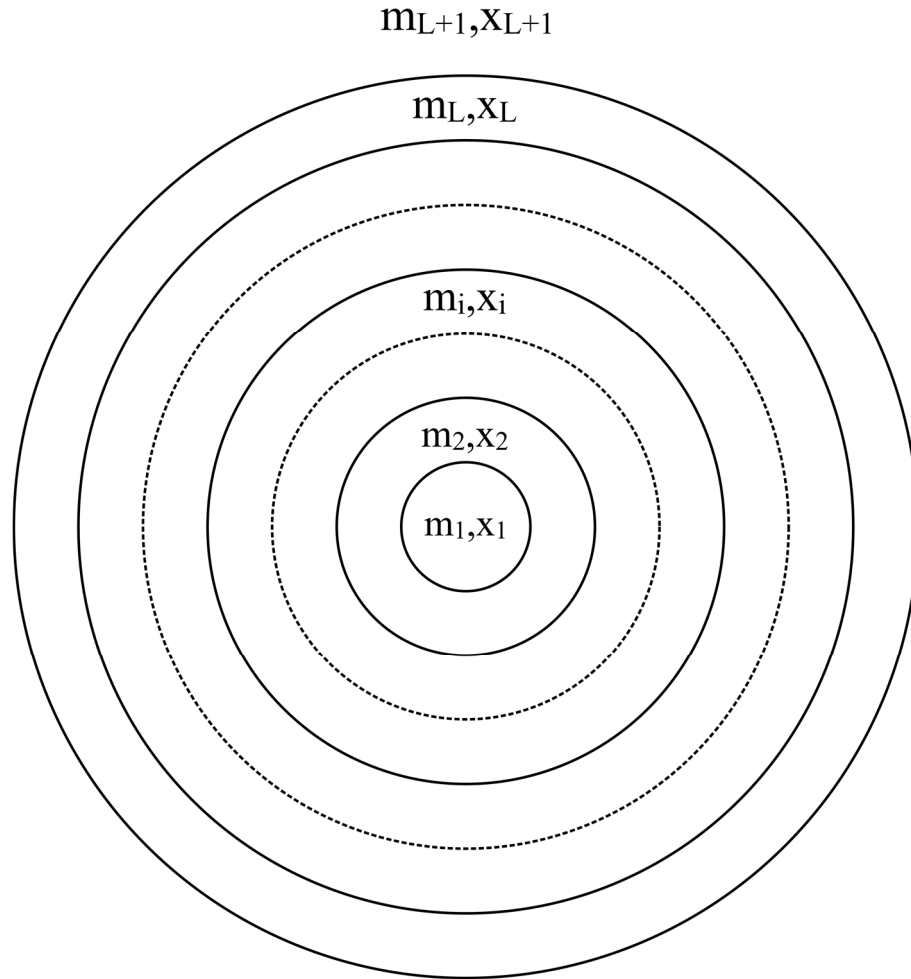


Figure 2-5: Multilayered concentric sphere particle geometry, adapted from [10].

If we assume the particle to be suspended in air we can take the relative index of the outermost layer,  $m_{L+1}$ , to be unity. We also will make the assumption that the permeability,  $\mu$ , is equivalent to the permeability of free space,  $\mu_0$ , everywhere. Now, if we were to excite an incident plane wave upon the multilayered sphere, we could express the field through a combination of inward and outward travelling waves. The inward travelling waves will be dictated by  $j_n(kr)$ , the spherical Bessel function of the first kind, while the outward travelling waves will be defined by the spherical Hankel

function of the first kind,  $h_n^{(1)}$  (kr), this is different from the typical choice in Mie scattering algorithms. We can express these travelling waves through the vector space spanned by  $\vec{N}$  and  $\vec{M}$  described in Section 2.2

$$E_{in} = \sum_{n=1}^{\infty} E_n \left[ c_n^{(l)} M_{o1n}^{(1)} - i d_n^{(l)} N_{e1n}^{(1)} \right] \quad (22a)$$

$$E_{out} = \sum_{n=1}^{\infty} E_n \left[ i a_n^{(l)} N_{e1n}^{(3)} - b_n^{(l)} M_{o1n}^{(3)} \right] \quad (22b)$$

From these definitions we can further explain the electric and magnetic fields in the 1<sup>th</sup> region of the sphere

$$E_l = \sum_{n=1}^{\infty} E_n \left[ c_n^{(l)} M_{o1n}^{(1)} - i d_n^{(l)} N_{e1n}^{(1)} + i a_n^{(l)} N_{e1n}^{(3)} - b_n^{(l)} M_{o1n}^{(3)} \right] \quad (23a)$$

$$H_l = -\frac{k_l}{\omega\mu} \sum_{n=1}^{\infty} E_n \left[ d_n^{(l)} M_{e1n}^{(1)} + i c_n^{(l)} N_{o1n}^{(1)} - i b_n^{(l)} N_{o1n}^{(3)} - a_n^{(l)} M_{e1n}^{(3)} \right] \quad (23b)$$

where  $E_n = i^n E_0 (2n+1)/n(n+1)$ ,  $\omega$  is the angular frequency, and  $M_{o1n}^{(j)}$ ,  $M_{e1n}^{(j)}$ ,  $N_{e1n}^{(j)}$ , and  $N_{o1n}^{(j)}$  ( $j=1,3$ ) are the vector harmonic functions with a radial dependence on  $j_n(k_l r)$  for  $j=1$  and  $h_n^{(1)}(k_l r)$  for  $j=3$ . Following Bohren and Huffman's treatment of light scattering in the core of the particle [13], we can see the fields expressed in the region,  $0 \leq r \leq r_1$  as

$$E_1 = \sum_{n=1}^{\infty} E_n \left[ c_n^{(1)} M_{o1n}^{(1)} - i d_n^{(1)} N_{e1n}^{(1)} \right] \quad (24a)$$

$$H_1 = \sum_{n=1}^{\infty} -\frac{k}{\omega\mu} E_n \left[ d_n^{(1)} M_{e1n}^{(1)} + i c_n^{(1)} N_{o1n}^{(1)} \right] \quad (24b)$$

The incident and scattered fields found in the surrounding medium can also be referred to in traditional Mie Theory expansions below.

$$E_i = \sum_{n=1}^{\infty} E_n \left[ M_{o1n}^{(1)} - i N_{e1n}^{(1)} \right] \quad (25a)$$

$$H_i = -\frac{k}{\omega\mu} \sum_{n=1}^{\infty} E_n \left[ M_{e1n}^{(1)} + i N_{o1n}^{(1)} \right] \quad (25b)$$

$$E_s = \sum_{n=1}^{\infty} E_n \left[ i a_n N_{e1n}^{(3)} - b_n M_{o1n}^{(3)} \right] \quad (25c)$$

$$H_s = -\frac{k}{\omega\mu} \sum_{n=1}^{\infty} E_n \left[ -ib_n N_{o1n}^{(3)} - a_n M_{e1n}^{(3)} \right] \quad (25d)$$

If we compare equations (23a) and (23b), (24a) and (24b), and (25a-d), we can infer that  $a_n^{(1)} = b_n^{(1)} = 0$ ,  $c_n^{(L+1)} = d_n^{(L+1)} = 1$ ,  $a_n = a_n^{(L+1)}$ , and  $b_n = b_n^{(L+1)}$ . We have already seen that we are able to obtain the scattering and expansion coefficients by applying the tangential boundary conditions in Section 2.2, however, now we need to implement a recursive function to solve for each layer of the sphere as we travel outwards from the core. This is achieved by utilizing the following definitions,

$$D_n^{(1)}(z) = \psi'_n(z)/\psi_n(z) \quad (26)$$

$$D_n^{(3)}(z) = \zeta'_n(z)/\zeta_n(z) \quad (27)$$

$$R_n = \psi_n(z)/\zeta_n(z) \quad (28)$$

where  $\psi$  represents the Riccati-Bessel function of the first kind, and  $\zeta$  represents the Riccati-Bessel form of the Hankel function of the first kind. In traditional multilayered sphere scattering algorithms these ratios are directly calculated given a real material index and then used to find intermediary terms that recursively solve inside out, until the final scattering coefficients can be obtained. However, it is well documented that many of these values grow exponentially with an increasingly large complex argument leading to overflow errors. Additionally, subsequent calculations required by previous algorithm schemes lead to subtractions of near zero terms which can lead to major round-off problems when considering the case of a finely stratified or highly absorbing shell particle. This new approach differs in the calculation of these logarithmic derivatives,  $D_n^{(1)}$  will be calculated via a downward recurrence scheme starting with a given initial value,

$$D_{N_{max}+15}^{(1)}(z) = 0+0i \quad (29)$$

$$D_{n-1}^{(1)}(z) = \frac{n}{z} - \frac{1}{D_n^{(1)}(z) + \frac{n}{z}} \quad (30)$$

where  $N_{max}$  is a decided number of terms in the partial wave expansion that has been thoroughly explored through the work of Wiscombe [14]. Similarly,  $D_n^{(3)}$  is solved through an upward recursion presented in the paper, “Internal absorption cross sections in a stratified sphere” by D.W. Mackowski [15], that uses the previously calculated  $D_n^{(1)}$  values to begin an upward recursion to find the  $D_n^{(3)}$  values where  $z$  represents your complex argument,  $a+ib$ .

$$D_0^{(3)}(z) = i \quad (31)$$

$$\psi_0(z)\xi_0(z) = \frac{1}{2}[1 - (\cos 2a + i \sin 2a)e^{-2b}] \quad (32)$$

$$\psi_n(z)\xi_n(z) = \psi_{n-1}(z)\xi_{n-1}(z) \left[ \frac{n}{z} - D_{n-1}^{(1)}(z) \right] \left[ \frac{n}{z} - D_{n-1}^{(3)}(z) \right] \quad (33)$$

$$D_n^{(3)}(z) = D_n^{(1)}(z) + \frac{i}{\psi_n(z)\xi_n(z)} \quad (34)$$

These logarithmic derivative values of the Riccati-Bessel function can then be used to find a new term,  $Q_n^{(l)}$ , which represents a ratio of the two distinct Bessel functions, however this time the recursion will produce a separate series for each layer of the sphere. While the numerator and denominator comprised of  $R_n(z)$  is unbounded, the ratio of these values as seen in the factor  $Q_n$  is.

$$Q_n^{(l)} = \frac{R_n(z_1)}{R_n(z_2)} = \frac{\psi_n(m_l x_{l-1})/\xi_n(m_l x_{l-1})}{\psi_n(m_l x_l)/\xi_n(m_l x_l)} \quad (35)$$

The values  $z_1$  and  $z_2$  are the complex arguments  $m_l x_{l-1}$ , and  $m_l x_l$  respectively. Next, the values of  $H_n^a$  and  $H_n^b$  will be generated based off of  $Q_n$  and four G values which are defined in Equations (36-41).

$$H_n^a(m_l x_l) = \frac{G_2 D_n^{(1)}(m_l x_l) - Q_n^{(l)} G_1 D_n^{(3)}(m_l x_l)}{G_2 - Q_n^{(l)} G_1} \quad (36)$$

$$H_n^b(m_l x_l) = \frac{\tilde{G}_2 D_n^{(1)}(m_l x_l) - Q_n^{(l)} \tilde{G}_1 D_n^{(3)}(m_l x_l)}{\tilde{G}_2 - Q_n^{(l)} \tilde{G}_1} \quad (37)$$

$$G_1 = m_l H_n^a(m_{l-1} x_{l-1}) - m_{l-1} D_n^{(1)}(m_l x_{l-1}) \quad (38)$$

$$G_2 = m_l H_n^a(m_{l-1} x_{l-1}) - m_{l-1} D_n^{(3)}(m_l x_{l-1}) \quad (39)$$

$$\tilde{G}_1 = m_{l-1} H_n^b(m_{l-1} x_{l-1}) - m_l D_n^{(1)}(m_l x_{l-1}) \quad (40)$$

$$\tilde{G}_2 = m_{l-1} H_n^b(m_{l-1} x_{l-1}) - m_l D_n^{(3)}(m_l x_{l-1}) \quad (41)$$

With the new H values that we have calculated in a more numerically stable way we can now return to traditional multilayer Mie theory algorithms in obtaining the scattering coefficients through Equations (42) and (43).

$$a_n = A_n^{(L+1)} = \frac{[H_n^a(m_L x_L)/m_L + n/x_L] \psi_n(x_L) - \psi_{n-1}(x_L)}{[H_n^a(m_L x_L)/m_L + n/x_L] \xi_n(x_L) - \xi_{n-1}(x_L)} \quad (42)$$

$$b_n = B_n^{(L+1)} = \frac{[m_L H_n^b(m_L x_L) + n/x_L] \psi_n(x_L) - \psi_{n-1}(x_L)}{[m_L H_n^b(m_L x_L) + n/x_L] \xi_n(x_L) - \xi_{n-1}(x_L)} \quad (43)$$

With these scattering coefficients, we now have the ability to calculate the desired cross-sections, efficiencies, and mass extinction coefficients of multilayered spherical particles with complex valued indices of refraction. This adapted Mie theory proves to be a powerful tool when combined with a graphical user interface, and an efficient coding scheme to optimize user designs for optical filter applications. In Chapter 3, we will detail the implementation of this theory into the MATLAB™ coding environment and explain its functionality.

## Chapter 3

### CODING AND OPTIMIZATION OF MULTILAYERED SPHERICAL PARTICLES

#### 3.1 Custom Mie Code

A custom Mie code was developed to help facilitate the design of optical filters based on multilayered spherical particles. The code which has been attached as an appendix to this thesis, has three distinct branches that work together to allow users to better understand how the material choice, number of layers, and layer thicknesses contribute to a filter's overall performance. The three branches include a custom Mie coefficient solver, graphical user interface (GUI), and a multi-step optimizer. The custom Mie code was programmed in the MATLAB<sup>TM</sup> numerical computing environment, which was selected for its broad function library and extensive use in the fields of Engineering and Science. In order to generate the response of each multilayered particle, we need an effective and stable method for calculating the mass extinction coefficient, extinction efficiency, or scattering efficiency. The code responsible for the generation of the scattering coefficients and eventual extinction profiles is located inside the function "Optimal\_spheres\_FP".

##### 3.1.1 Optimal Spheres Function

Wang's aforementioned revised recursive algorithms for light scattering by a multilayered sphere has been incorporated into a function in this file, which will be responsible for providing the stable and efficient calculation of the scattering coefficients. However, the "Optimal\_spheres\_FP" file as a whole will work in a loop to use slew of user inputs and stored material properties to create descriptive arrays for the particle designs built in the GUI that are being examined during the optimization

process. These descriptive arrays will serve as inputs to the “calcmie\_coeff\_FP” function which will be directly responsible for calculating the scattering coefficient for the design based on those arrays. Then the entire process will repeat, slightly modifying the descriptive arrays built for the design as the wavelength is iterated to the next value.

This loop has many complex steps, but initially the function takes in an array,  $x$ , comprised of layer thicknesses in micron. From  $x$ , the rest of the program can gather the total number of layers for the design. The function also pulls in important design properties such as the complex index of refraction matrix for all of the particles incorporated materials in the wavelength band of interest, material densities, and a hollow or solid core designation. These variables are primarily set in the GUI through user input, and will be discussed in subsequent sections.

With  $x$ , the function builds a new array,  $r$ , which adds the core radius and layer thicknesses to build a single dimensional array holding the radii for an equivalent concentric spheres model that will be adapted from the shell geometry. This approach mirrors that of Wang’s initial setup outlined in Chapter 2. Next, the mass of the particle is calculated by recalling the stored density and radii values inside of a simple set of equations. After the mass of the particle is stored in memory, another array,  $ns$ , is built by iterating through each layer and assigning an index value given a specific wavelength and material designation. The values used for the index of refraction interpolation were taken from the *Handbook of Optical Constants of Solids* [16]. Once the index array,  $ns$ , and radii array,  $r$ , have been built at a particular wavelength “calcmie\_coeff\_FP” is called. This function takes in both the  $ns$  and  $r$  arrays at a given wavelength, the index of the surrounding media (typically taken to be free space, or  $n_m = 1$ ), and a series of option parameters which are then used in the recursive algorithm scheme to return the

scattering coefficients,  $a_n$  and  $b_n$ , for that particle design. The details of this function will be discussed in the next section, but for now let's continue to examine the parent function. After obtaining the scattering coefficients, the function calculates an extinction efficiency by substituting their values into Equations (18) and (19) as seen in Figure 3-1, and indexes their values into two new arrays  $Q_{ext}$  and  $Q_{sca}$ .

```
[ an, bn ] = calcmie_coeff_FP( r, ns, nm, wavelengthopt(ii),...
    'ConvergenceFactor', conv, ...
    'TotalField', tf_flag, ...
    'Cartesian', cc_flag);

n=1:length(an);
a=max(r);
k=2*pi./wavelengthopt(ii);
Qext(ii)=2./(k*a).^2*sum((2*n+1).*real(an+bn));
global Qsca;
Qsca(ii) = 2./(k*a).^2*sum((2*n+1).*(abs(an).^2)+(abs(bn).^2));
```

Figure 3-1: Calculation of extinction and scattering efficiencies from the “Optimal\_spheres” function

After storing the extinction and scattering efficiencies at the current wavelength, the function iterates through to the next wavelength step for which a new index array must be calculated. This loop continues, eventually generating a full array of scattering and extinction efficiencies for the entire wavelength band. It is important to note that because this function will be used to define the figure of merit for each particle design in the optimizer, the step size of the wavelength band may be rather large. The large step size is chosen in order to allow the solver to quickly quantify the general shape of the profile so that the optimizer can determine a representative function value quickly before iterating to the next design. A much smaller wavelength step will be used in the

function “Optimal\_spheres\_test” which will be used to plot the extinction profile of the optimal design after completing a sufficient optimization requirement. Following the for-loop iteration, the efficiency arrays, Qsca and Qext are used to calculate the mass extinction coefficient, “alpha”, and scattering cross-section, “sigma\_sca”.

The function value, F, returned by the file is based on a user defined optimization scheme in order to quantify the current design’s performance in a given application which can then be passed along to the overlaying optimizer. Figure 3-2 displays a simple optimization scheme developed inside of the “Optimal\_spheres\_FP” function that seeks to promote designs with low extinction about a center wavelength while encouraging the highest possible average extinction outside of that localized dip. The full optimization details will be discussed in Section 3.3.

```

if graphtype == 'ME'
    variable = alpha_opt;
elseif graphtype == 'SE'
    variable = Qsca_opt;
elseif graphtype == 'QE'
    variable = Qext_opt;
elseif graphtype == 'SC'
    variable = sigma_sca_opt;
end

if (strcmp(FilterSelect,'PB') == 1)
    buffer = round(length(variable)/12); % buffer variable used to isolate points inside dip from outside extinction
    dip = 0;
    wall = 0;
    counter = 0;
    for i = 1:length(variable)
        if (i > ((length(variable)/2) - buffer) && (i < (length(variable)/2) + buffer)) ...
            % If the point falls inside the buffer zone
            dip = dip + variable(i); % add the values to calculate an effective dip value
        else
            if(variable(i) < .2)
                bad = bad + 1;
            end
            counter = counter + 1; % count number of values contributing to wall variable
            wall = wall + variable(i); % add extinction/scattering value at point outside of dip
        end
    end
    average = wall / counter; % average extinction/scattering value outside of dip
    F = ((variable(Imin).^3) / average); % final function value used returned to optimizer

```

Figure 3-2: Excerpt of “Optimal\_spheres” function assigning a function value for an optimal pass-band filter device.

After executing the entire function, the design parameters including a modified  $r$  array are sent back to the GUI with a specific layer thickness indicated for optimal filter performance.

### 3.1.2 Custom Mie Coefficient Solver

As mentioned previously, “`calcmie_coeff_FP`” is an adapted MATLAB™ function that will be used to implement Wang’s revised recursive algorithm for the calculation of the scattering coefficients of finely stratified and highly absorbing multilayered spherical particles. The function takes in the radii array,  $r$ , and the index array,  $n_s$ , and the current wavelength step. From these values the function evaluates the wavenumber in the surrounding medium,  $k$ , the particle’s size parameter,  $x$ , and the relative refractive index,  $m$ , which is simply the index array,  $n_s$ , divided by the index of the surrounding medium,  $n_m$ . The function then checks to see if the sphere is homogeneous, or multilayered, if it is multilayered, as is usually the case with our design principles, it will call a secondary function, “`expcoeff_mie_strat_FP`”. This new function will be responsible for calculating the expansion coefficients for the scattering of a stratified sphere, and inside are the adapted functions created based upon Wang’s algorithm.

The first calculation made in the “`expcoeff_mie_strat_FP`” file is in evaluating the truncation number,  $M$ . The truncation number is an important variable that looks at the value of the size parameter and relative refractive index of each concentric sphere, and from that information it estimates the necessary size of the partial wave expansion [14]. Figure 3-3 shows the implementation of the truncation number calculation in my code, originally expressed by Wiscombe.

---

```

%% Calculate truncation number
if(x(end)<=8 && x(end)>=.02)
    Mstop = ceil(conv*(x(end) + 4*x(end)^(1/3) + 1));
elseif (x(end)<4200 && x(end)>8)
    Mstop = ceil(conv*(x(end) + 4.05*(x(end)^(1/3)) + 2));
else
    Mstop = ceil(conv*(x(end) + 4*(x(end)^(1/3)) + 2));
end

M = round(Mstop) + 15;

```

Figure 3-3: MATLAB™ implementation of Wiscombe’s truncation number

Finally, the function initializes the necessary matrices for holding the numerous variables and initial values which will be called during the execution of the Wang’s recursive algorithm. The actual execution of the algorithm is shown in Figure 3-4, performed by the function “FindAnBn”, which is called in the “expcoeff\_mie\_strat\_FP” function, a function I have written to implement Wang’s theory.

```

1  function [an,bn] = FindAnBn(M,x,ns)
2  -   global Han;
3  -   global Hbn;
4  -   global Psi;
5  -   global Xi;
6  -   persistent mL;
7  -   persistent xL;
8  -   persistent Han_an;
9  -   persistent Hbn_bn;
10 -   persistent Psi_dummy;
11 -   persistent Xi_dummy;
12
13 -   an = zeros(1,M);
14 -   bn = zeros(1,M);
15 -   mL = ns(end);
16 -   xL = x(end);
17 -   FindHan(M,1,x,ns)
18 -   Han_an = Han(end,:);
19 -   FindHbn(M,1,x,ns);
20 -   Hbn_bn = Hbn(end,:);
21 -   FindPsi(M,1,x);
22 -   Psi_dummy = Psi;
23 -   FindXi(M,1,x);
24 -   Xi_dummy = Xi;
25
26 -   for n = 1:M
27 -       an(n) = (((((Han_an(n+1) / mL) + ((n)/xL)))*Psi_dummy(n+2)) - Psi_dummy(n+1)) ...
28 -           / (((((Han_an(n+1) / mL) + ((n)/xL)))*Xi_dummy(n+2)) - Xi_dummy(n+1));
29
30 -       bn(n) = (((((mL * Hbn_bn(n+1) + ((n)/xL)))*Psi_dummy(n+2)) - Psi_dummy(n+1)) ...
31 -           / (((((mL * Hbn_bn(n+1) + ((n)/xL)))*Xi_dummy(n+2)) - Xi_dummy(n+1));
32 -   end
33
34 - end

```

Figure 3-4: MATLAB™ adaptation of Wang’s recursive algorithms

In the “FindAnBn” function a carefully selected sequence of sub-functions is called to recursively populate the logarithmic derivatives of the Riccati-Bessel functions. Inside of the function “FindHan” and “FindHbn” hold the functions that generate  $D_n^{(1)}$ ,  $D_n^{(3)}$ ,  $Q_n^{(1)}$ , and all four G functions described in Section 2.4. The larger algorithm is then pieced together through an implementation of Equations (42) and (43), ultimately returning the scattering coefficients  $a_n$  and  $b_n$ . This calculation will occur thousands of times as the overall program loops through the wavelength array. The

scattering coefficients derived at each wavelength will be used to back out a single curve for the efficiencies, cross-sections, and mass extinction coefficients seen in later graphs.

```

1 function [] = FindHan(M,l,x,ns)
2 - global Dn1;
3 - global Dn3;
4 - global Qn;
5 - global G1;
6 - global G2;
7 - global Han;
8     if( l == 1)
9         FindDn1(M,M,(ns(l)*x(l)),l,l);
10        Dn1_Han1 = Dn1;
11        Han(1,:) = Dn1_Han1(1,:);
12        l = l+1;
13    end
14    if( l <= numel(x) && l ~= 1)
15        FindG1G2(M,x,l,ns);
16        G1_Han = G1;
17        G2_Han = G2;
18        FindQn(M,l,l,x,ns);
19        Qn_Han = Qn;
20        FindDn1(M,M,(ns(l)*x(l)),l,l);
21        Dn1_Han = Dn1;
22        FindDn3(M,l,(ns(l)*x(l)),l);
23        Dn3_Han = Dn3;
24        for n = 1:M+16
25            Han(1,n) = ((G2_Han(1,n) * Dn1_Han(1,n)) - (Qn_Han(1,n) * G1_Han(1,n) * Dn3_Han(1,n)))...
26            / (G2_Han(1,n) - (Qn_Han(1,n)*G1_Han(1,n)));
27        end
28        l = l+1;
29        FindHan(M,l,x,ns);
30    else
31        return;
32    end

```

Figure 3-5: MATLAB™ adaptation of Wang’s recursive Han function (Equation 36).

### 3.2 Graphical User Interface

In order to take full advantage of our newfound ability to generate the extinction profiles of multilayered spherical particles with complex indices of refraction, I developed a graphical user interface using the tools provided by the MATLAB™ guide software. This interface allows users unfamiliar with the complex theory behind the calculations to easily modify a design setup and obtain an accurate summary of the particle’s performance in a given wavelength band. When designing the GUI, I decided

to group the user inputs into two major sections titled “Design Parameters” and “Simulation Setup”.

### **3.2.1 Design Parameters**

In the “Design Parameters” section of the GUI, users are able to select the desired filter type, along with specific requirements they would like to impose in that filter’s design. In this case either a pass-band filter centered around the pass-band wavelength input, or a broad stop-band filter can be chosen from the available options. This input determines the appropriate function value algorithm calculated in the “Optimal\_spheres\_FP” function. For example, when a user selects the narrow pass-band filter option, the function value will want to minimize extinction at the pass-band wavelength, while maximizing it outside of the pass-band. A broad stop-band filter would conversely aim to maximize the extinction at all areas of the band from the start to stop wavelength. Next, the user can input the total number of layered media on top of the core. This is valuable, because the user may have a practical limitation imposed by the fabrication equipment that dictates the maximum number of layered media that can be deposited on a spherical core given its size and will want to limit optimization to this complexity. Another drop-down menu allows the user to select a material type for the core, and each layer. The layers are represented by two variables shown as Material 1 and Material 2. These materials will be alternated starting with a layer of Material 1 directly on top of the core material. This design choice allows high and low index alternating layers to be easily generated to simulate the interference effects found in thin-film optical filters. Once selected, a large array of the material’s complex index will be stored into memory. The wavelength band of interest can be dictated by user entry into the start and stop wavelength text boxes, and doing so will begin a background

interpolation of the selected material properties to ensure a consistently dense grid will be available when calculating the scattering coefficients at the specific subset of data points within the previously existing index array. Finally, users may input a specific core radius and layer thicknesses in order to manually select an initial value for optimization, or to simply evaluate it. Figure 3-6 below depicts the “Design Parameter” section of the GUI.

The screenshot shows the 'Design Parameters' section of the GUI. It contains the following fields and values:

Parameter	Value	Unit
Select Filter Type	Narrow pass-band filter	
Core radius	1	um
Select Number of Layers	3	
Layer Thicknesses	0.251341	um
Core	Silicon Dioxide	um
Material 1	Silicon	um
Material 2	Silicon Dioxide	um
Start Wavelength	1	um
Stop Wavelength	3	um
Window Frequency	2	um
Layer Thicknesses (Material 2)	N/A	um
Layer Thicknesses (Material 1)	N/A	um

Figure 3-6: Design parameter sub-section of the Multilayered Spherical Optical Filter GUI

### 3.2.2 Simulation Setup

The next field for user entry inside the GUI is the “Simulation Setup” section. In this section users will be able to decide the simulation and optimization types, graph the resulting profile, and reset all user inputs. Most often, the user will begin an optimization from an initial design condition, or produce a graph of a specific design input, however if the user does not have a starting value, an initial starting value will be created based upon the application that will determine initial core and layer sizes. The drop down labeled “Simulation Type” allows users to decide which variable they would like to optimize for, and subsequently plot on the axes located to the right. The variable options include the particle extinction efficiency, scattering efficiency, scattering cross-section, or mass extinction coefficient as a function of wavelength. There is a checkbox for users to allow the optimizer to modify the core size if it is not fixed, and in the pattern search checkbox the user can manually switch optimization functions. Finally, the “Run” and “Graph” buttons start the optimization and plot the results respectively.

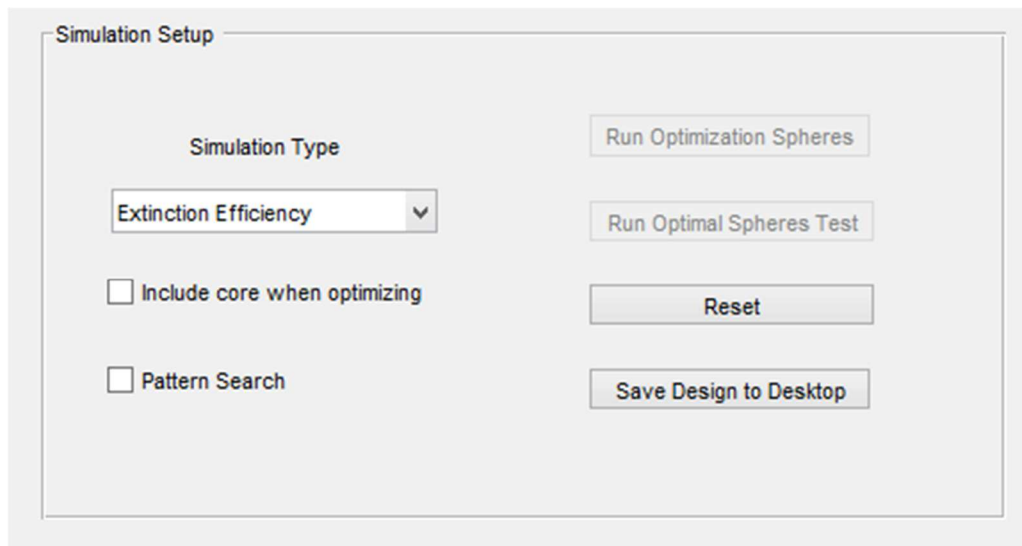


Figure 3-7: Simulation setup section of the Multilayered Spherical Optical Filter GUI.

To summarize, these two sections work together with two built-in optimization functions, allowing users to quickly input and modify their designs and plot their selected variable of the particle in the axes provided in the GUI. This tool will help to design and discover new multilayered particle applications that can easily be modified to facilitate specific user requirements. An example GUI simulation for a narrow pass-band filter centered around a 2 $\mu\text{m}$  wavelength is shown below in Figure 3-8.

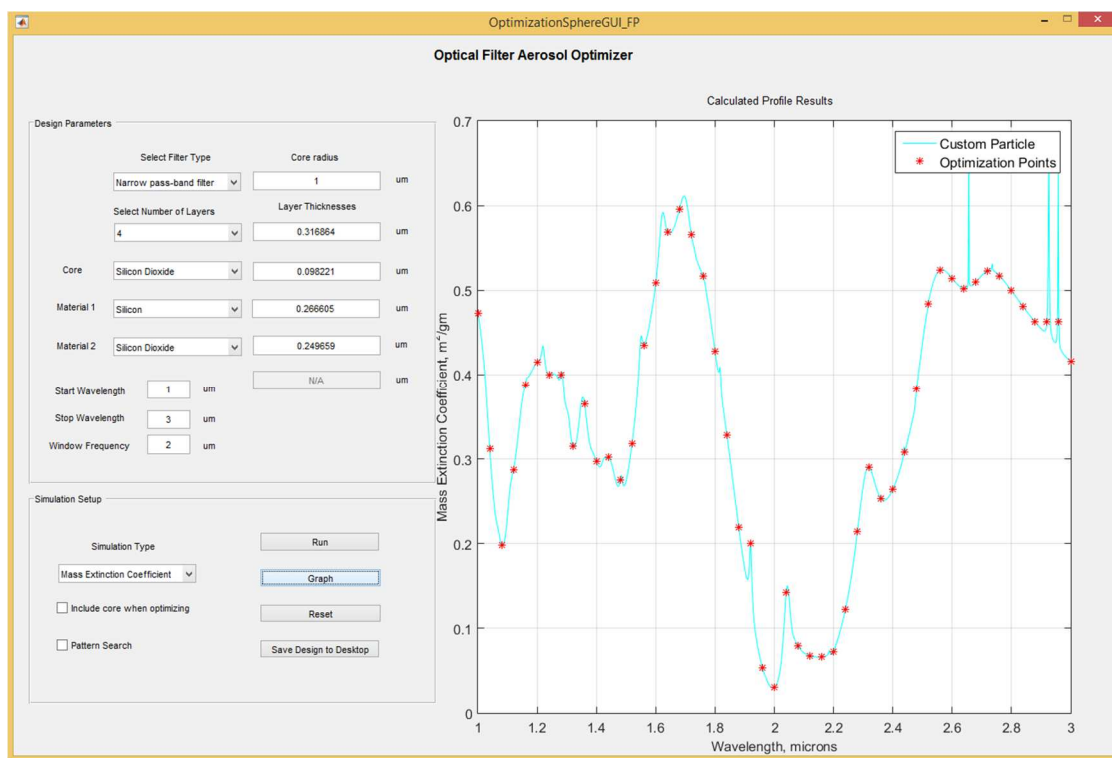


Figure 3-8: MATLAB™ GUI for multilayered spherical optical filter code.

The axes shown in the figure above display two curves, a solid blue curve representative of the final simulation of the particle, and a curve consisting of a number of starred red points. The solid blue curve has a very small wavelength step to provide the user with

better resolution when examining the filter's performance. It is therefore calculated only at the completion of optimization. The starred curve is displayed to show the user which points are being seen by the optimizer contributing to its function value. This allows the user to modify the density of the optimization wavelength to balance speed and efficient characterization of the filter during the process.

### **3.3 Optimization Code**

The optimization code in this program works to minimize a function value,  $F$ , that is generated based on filter type or application requirements and is user-defined. An example of a simple function value algorithm was given in Figure 3-2. Inside the "Optimal\_spheres\_FP" function. The function compares the chosen output figure of merit (mass extinction, scattering efficiency, etc.) to the desired value dictated by the design's application in order to assign a numerical value to that variable's profile over the wavelength band. Since both of the two optimization codes work to find the lowest possible function value, the algorithm needs to be developed with minimization in mind. If a broad stop-band filter is desired the user should create a function value algorithm in which the average of the particle extinction efficiency over the band is located in the denominator of the function, therefore, the higher the extinction across the band, the smaller the function value will become and hence the better chance that design will have of being chosen as the optimal particle design. Both optimization types display a current and best function value, which will indicate the most recently evaluated design's function value compared to the lowest (or best) function value it has found thus far. The two optimization functions used in this program are "simulannealbnd.m" and "patternsearch.m". Both functions are built in to the MATLAB™ global optimization toolbox.

### **3.3.1 Simulated Annealing**

The bounded simulated annealing optimization is the first of the two possible optimizations that will occur when searching for a particle design. The user will enter the design constraints before pressing run, which will begin by evaluating the given initial design and obtaining its function value before running the simulated annealing search algorithm to choose its next design. The simulated annealing algorithm is known as a threshold algorithm and can be useful in a wide range of problems. It exhibits a stochastic factor in its iteration, where the path it takes may be estimated through probability, but cannot be defined outright. It allows the program to search through seemingly random layer thicknesses while offering the user the ability to bound specific outputs to upper and lower limits [17]. For example, if a user would like to optimize for a particle with a fixed core size, number of layers, and maximum layer thickness, it can randomly iterate through some of the design possibilities that fall within those criteria. This allows for an effectively broad search across the numerous design possibilities if given enough time to acquire a design with a sufficiently low function value. The progress made by the optimizer is displayed in a separate pop-up window after the user initiates the function in the GUI. Figure 3-9 displays the user's view of the simulated annealing optimization in progress.

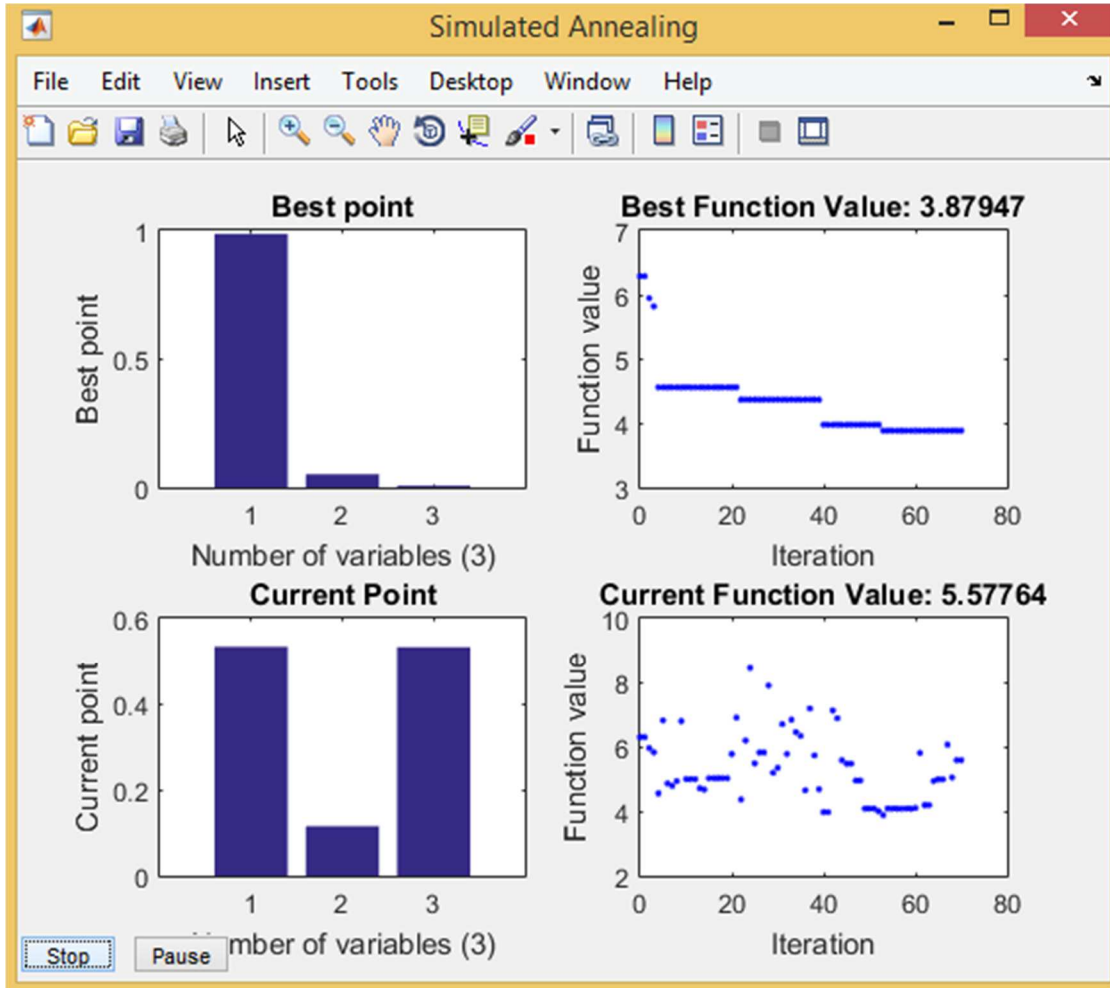


Figure 3-9: In progress view of simulated annealing optimization including best (top) and current (bottom) designs.

The simulated annealing optimization is capable of rapidly testing different design options usually leading to thousands of optimizations in a matter of minutes, when the user is satisfied with the best function value seen in the optimizer's interface they can move on to the second optimization function by pressing stop, allowing the best design's layer thicknesses to pass back into the GUI before checking the "Pattern Search" checkbox.

### **3.3.2 Pattern Search**

After the simulated anneal optimization is complete and the pattern search checkbox is selected, and the program begins the second optimization. The pattern search algorithm begins at an initial value based on the output of the simulated annealing optimization and then builds a mesh that extends equally in all directions if the binding constraints permit it [18]. The function value at each of the extended points of the mesh are evaluated until a lower function value is found, if successful the algorithm will move to that point and modify the mesh size, most often by multiplying it by a constant before repeating the process. If no lower function value is found the algorithm, then reduces the mesh size by multiplying by a constant less than 1. This continues until an “optimal” function value has been found and the mesh searching no longer produces a reduction in function value. This optimization provides more utility as an efficient way to obtain the local minimum of the design that produced the lowest function value in the more sporadic simulated annealing search. Upon termination of pattern search, your final layer thicknesses will be placed into the text boxes displayed in the design parameter section of the GUI. At this time the user can click the “Graph” button to display the results. The results can be graphed alone, compared to a previous design, or overlaid with the optimization points to better understand why your optimizer chose that profile as the optimum design.

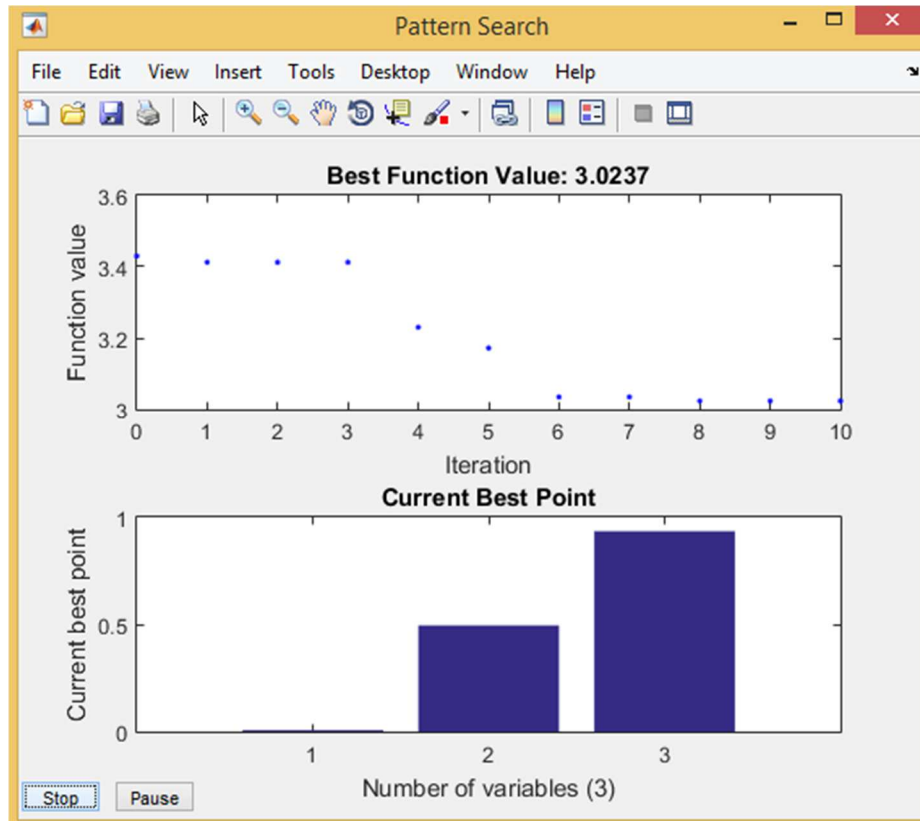


Figure 3-10: In progress view of the Pattern Search optimization including best (top) and current (bottom) designs.

These two optimization schemes work together well to sufficiently search through the possible filter designs when determining the geometries required to facilitate a user's needs. With these tools the design of multilayered spherical optical filters will become much faster and efficient. Now that the theory and code behind the process has been discussed we can move on to a few examples of designing, optimizing, and evaluating practical optical filters in Chapter 4.

## Chapter 4

### RESULTS AND APPLICATIONS

#### 4.1 Single Particle Simulation for MWIR Stop-Band Filters

When designing a stop-band filter in the MWIR ( $\lambda = 8\text{-}12\mu\text{m}$ ) it is important to first outline the application requirements before making a determination of an ideal geometry or material choice in the optimization code. In this instance we wish to create a high mass extinction filter that will impede the transmission of incident energy between the wavelengths of 8 and  $12\mu\text{m}$ . Since the filter is designed to be deployed as an aerosol, the particles must be light enough to maintain a suspension in air for a sufficient period of time. Aluminum was chosen due to its high absorption in the MWIR and relatively low density ( $2.70\text{ g/cm}^3$ )

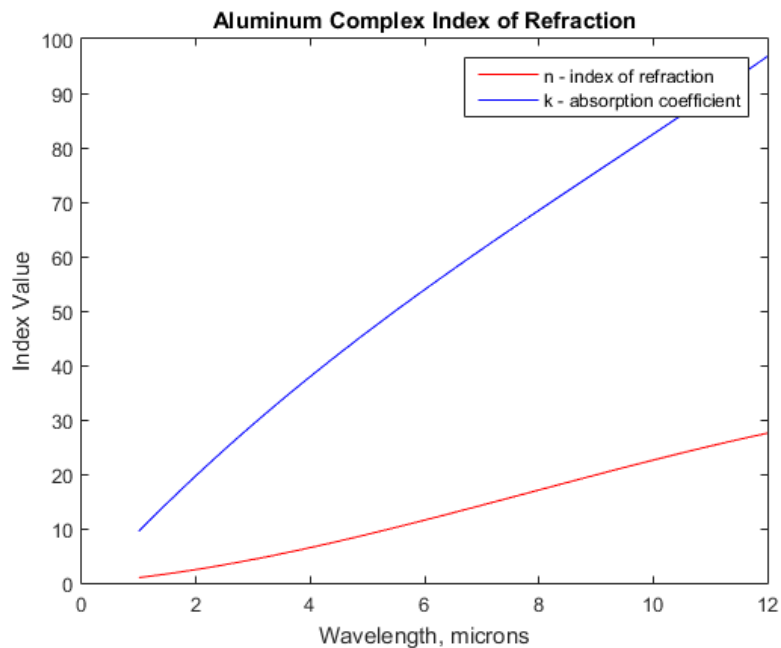


Figure 4-1: Aluminum complex index of refraction plotted against wavelength in the mid-wave infrared [16].

In order to satisfy the weight requirement of an aerosolized filter a hollow-core design will be pursued. Obviously, the trade-off of this design choice would primarily be particle durability, and in order to preserve the particle's integrity during dispersal a minimum wall thickness of 20nm will be imposed on the bounded optimizers. Figures 4-2 through 4-4 overview the entire simulation process from initial user input to the generated filter profile.

The image shows a software interface divided into two main sections: "Design Parameters" and "Simulation Setup".

**Design Parameters:**

- Select Filter Type:** Broad stop-band filter (dropdown)
- Core radius:** 5 um (input field)
- Select Number of Layers:** 1 (dropdown)
- Layer Thicknesses:** 0.025 um (input field)
- Core:** Air (dropdown)
- Material 1:** Aluminum (dropdown)
- Material 2:** Silicon (dropdown)
- Start Wavelength:** 8 um (input field)
- Stop Wavelength:** 12 um (input field)
- Window Frequency:** 1 um (input field)

**Simulation Setup:**

- Simulation Type:** Mass Extinction Coefficient (dropdown)
- Include core when optimizing
- Pattern Search
- Buttons:** Run, Graph, Reset, Save Design to Desktop

Figure 4-2: Initial user GUI input for high mass extinction aluminum hollow sphere design.

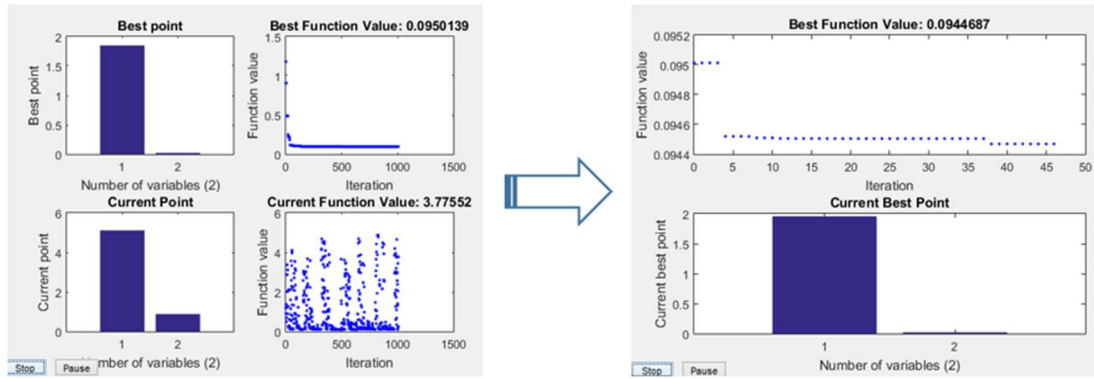


Figure 4-3: Results of simulated annealing and pattern search optimization processes for MWIR broad stop-band filter.

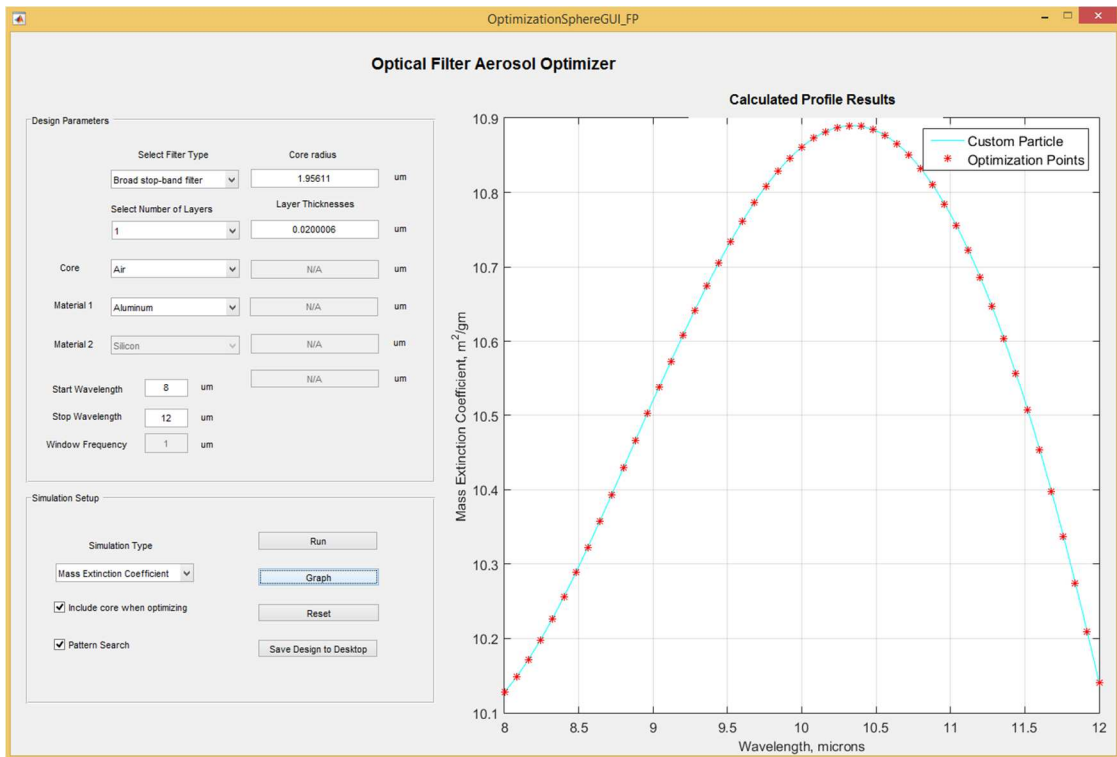


Figure 4-4: Resulting filter profile of optimized MWIR aluminum hollow-core stop-band filter.

The function value of the design dropped from an original value of 1.3 to a final value of .0944, indicating that our initial particle geometry of an aluminum hollow particle with a 5-micron radius and 25 nanometer wall thickness could be greatly improved upon. The final geometry of the optimized particle has a 1.95-micron radius and wall thickness of 20 nanometers. The fact that our optimized wall thickness came out to be our lower boundary makes sense, as the absorption properties of the particle contributed by the aluminum remains largely unchanged with thicknesses of at least 5 nanometers before dropping significantly. Therefore, if we continued to decrease our wall thickness as the optimizer decided to do we would be cutting mass without sacrificing particle extinction properties, however since the restrictions imposed to our particle integrity requires a 20 nanometer wall thickness our optimizer continued to reduce the wall thickness until it conflicted with the bounded conditions. With this design we are able to achieve a relatively large mass extinction coefficient of 10-11  $\text{m}^2/\text{g}$ , which peaks about the middle of our wavelength band. Through correspondence with other researchers and engineers these high mass extinction values seem to be at least an order of magnitude higher than most other commonly used extinction aerosols [19-21]. Overall, this simulation was very successful in producing a promising particle design.

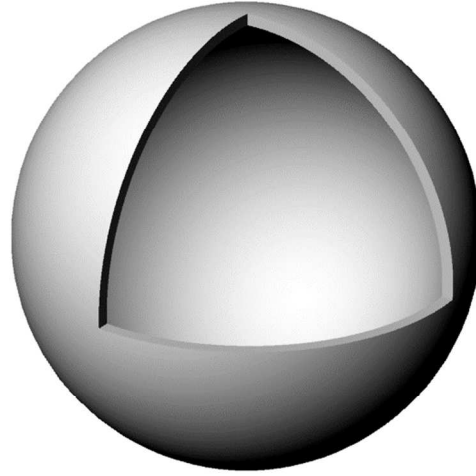


Figure 4-5: Render of MWIR stop-band filter (20-nm thick aluminum hollow-shell).

#### **4.2 Single Particle Simulation for SWIR Pass-Band Filter**

The second device we aim to design is a narrow pass-band filter in the short wave infrared spectrum ( $\lambda = 1\text{-}3\mu\text{m}$ ). This application requires us to use materials that have low absorption coefficients in the pass-band, while providing a low enough density such that the particle can stay suspended even without a hollow-core design. The design instead will attempt to recreate an alternating high and low index thin-film reflector with a pass-band centered around the middle of the SWIR range ( $2\mu\text{m}$ ). The materials used to construct the thin-film reflector will be silicon ( $n \approx 3.44$ ) and silicon dioxide ( $n \approx 1.43$ ), both materials exhibit relatively low absorption coefficients in the SWIR band, while maintaining a high index contrast necessary for creating the interference effects

of the filter, additionally their densities are low enough to achieve suspension if the core size is sufficiently small.

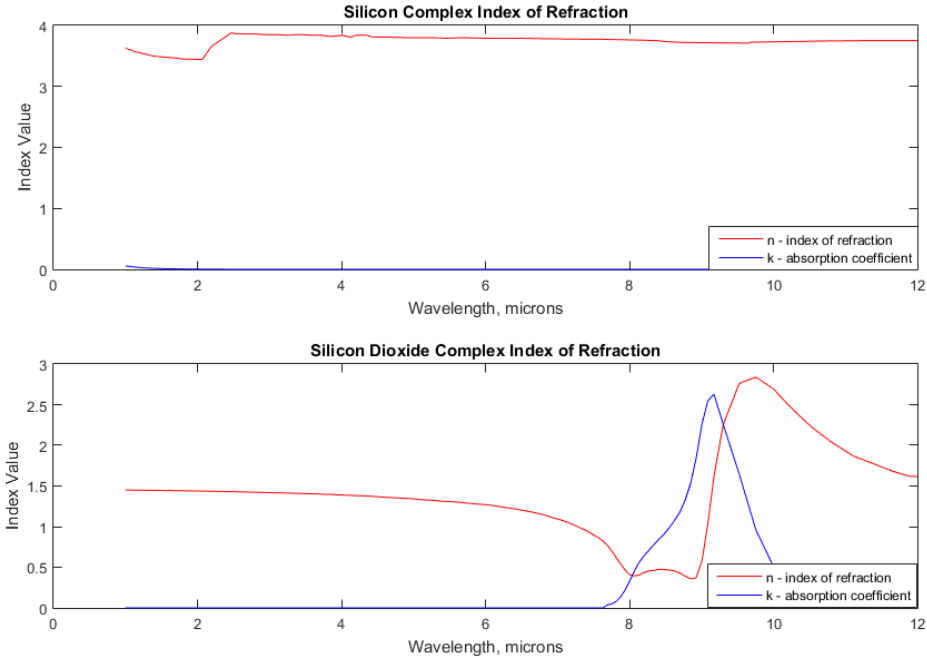


Figure 4-6: Complex index of refraction for silicon and silicon dioxide for  $\lambda = 1\text{-}12\mu\text{m}$  [16].

Another requirement of the thin film reflector dictates that the design must start and end with the higher index material [3]. For these reasons we have chosen a solid-core silicon dioxide particle with an odd number of alternating silicon/silicon dioxide layers. In order to keep particle mass down we have restricted the core to a maximum radius of 3 microns. With these constraints in mind, the same process was followed as outlined in the broad stop-band filter to optimize our design. An image of the initial user inputs for the optimization are shown below in Figure 4-7

**Design Parameters**

Select Filter Type	Core radius
<input type="text" value="Narrow pass-band filter"/>	<input type="text" value="2"/> um
Select Number of Layers	Layer Thicknesses
<input type="text" value="3"/>	<input type="text" value="0.25"/> um
Core	<input type="text" value="0.25"/> um
Material 1	<input type="text" value="0.25"/> um
Material 2	<input type="text" value="N/A"/> um
Start Wavelength	<input type="text" value="1"/> um
Stop Wavelength	<input type="text" value="3"/> um
Window Frequency	<input type="text" value="2"/> um

**Simulation Setup**

Simulation Type	<input type="button" value="Run"/>
<input type="text" value="Mass Extinction Coefficient"/>	<input type="button" value="Graph"/>
<input checked="" type="checkbox"/> Include core when optimizing	<input type="button" value="Reset"/>
<input type="checkbox"/> Pattern Search	<input type="button" value="Save Design to Desktop"/>

Figure 4-7: Initial user GUI input for narrow pass-band filter design.

Here we can see that we have allowed the optimizer to make an initial simulation for a 2-micron radius, 3-layered particle with a silicon dioxide core and alternating silicon and silicon dioxide layers. The optimization took about 5 minutes to find a better design and ended up reducing the function value by a factor of 100. The exact steps taken by the optimization steps can be seen below.

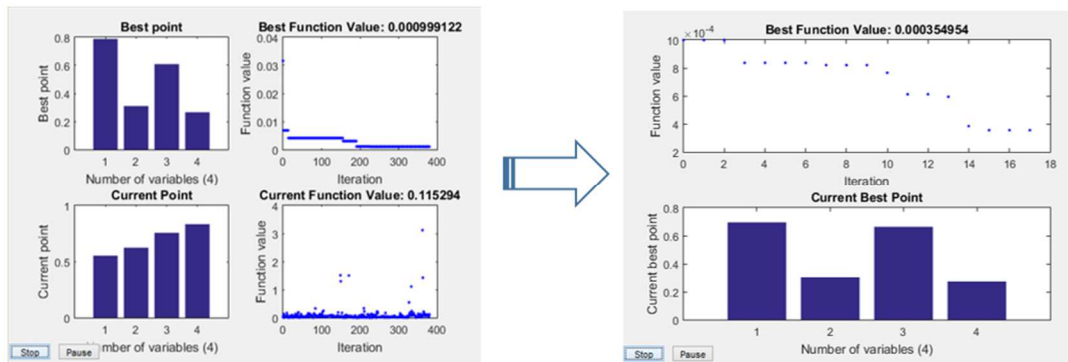


Figure 4-8: Results of simulated annealing and pattern search optimization processes for SWIR narrow pass-band filter

The final particle design resulting from the optimization is a multilayered Si/SiO<sub>2</sub> particle with a core diameter of 1.39 microns and layer thicknesses of 302, 664, and 273 nanometers respectively. The profile of the filter displays a narrow dip in extinction about the center of the SWIR band as intended with a relatively high mass extinction over the rest of the band.

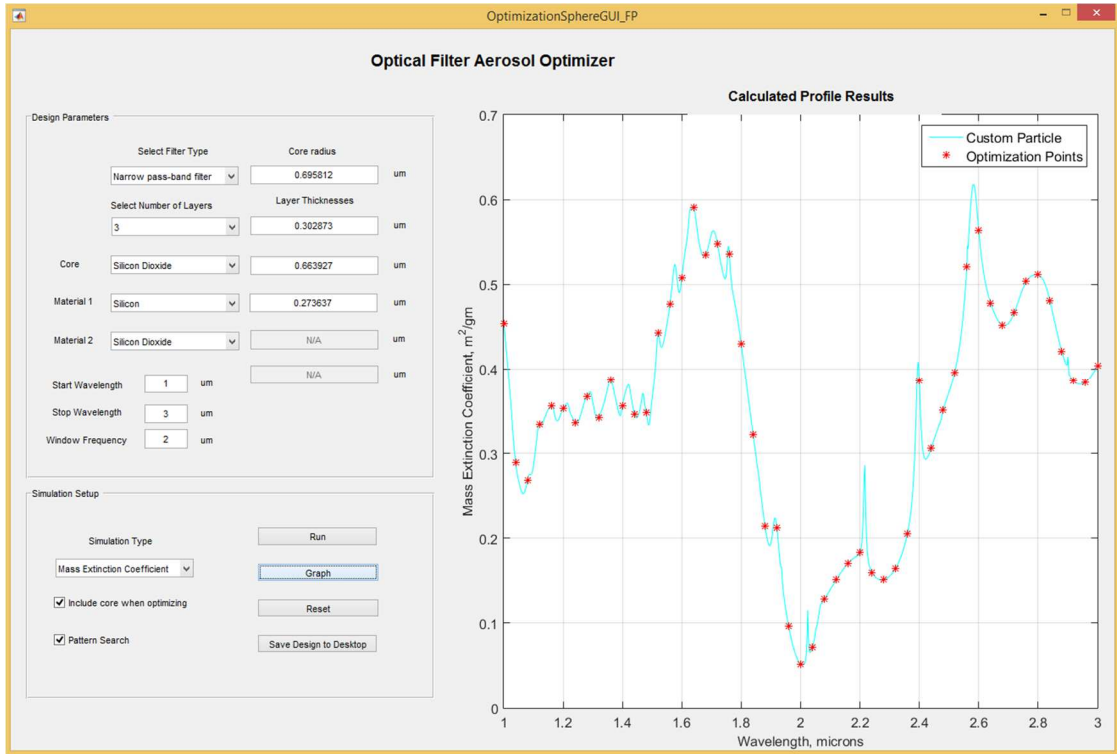


Figure 4-9: Resulting filter profile of optimized SWIR Si/SiO<sub>2</sub> pass-band filter.

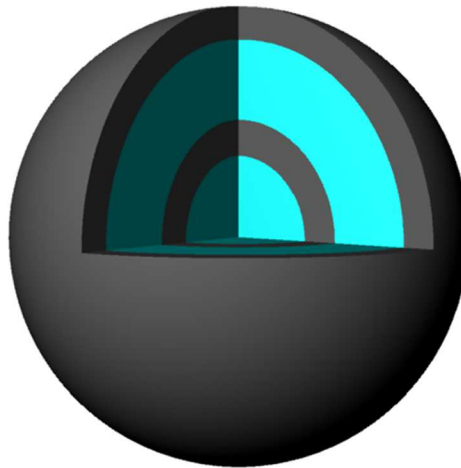
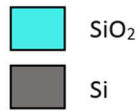


Figure 4-10: Render of optimized SWIR pass-band filter design.

Overall the adaptation of the thin film reflector onto the spherical particle, while not perfect, did help to create sharp peaks in the extinction curves for narrow-band filters, and I believe with further work the designs can be improved to create more unique, user-defined filter profiles.

### 4.3 Validation of Results

To confirm the validity of my results, I performed a few comparisons between the custom developed Mie code and Lumerical™, a commercially available 3D FDTD-method Maxwell solver. As an initial test to see how both programs would handle the solving of a multilayered, complex valued spherical particles I simulated a 2-micron diameter silicon dioxide particle with a 20 nanometer aluminum shell to output the mass extinction of the particle over the SWIR band ( $\lambda = 1\text{-}3\mu\text{m}$ ).

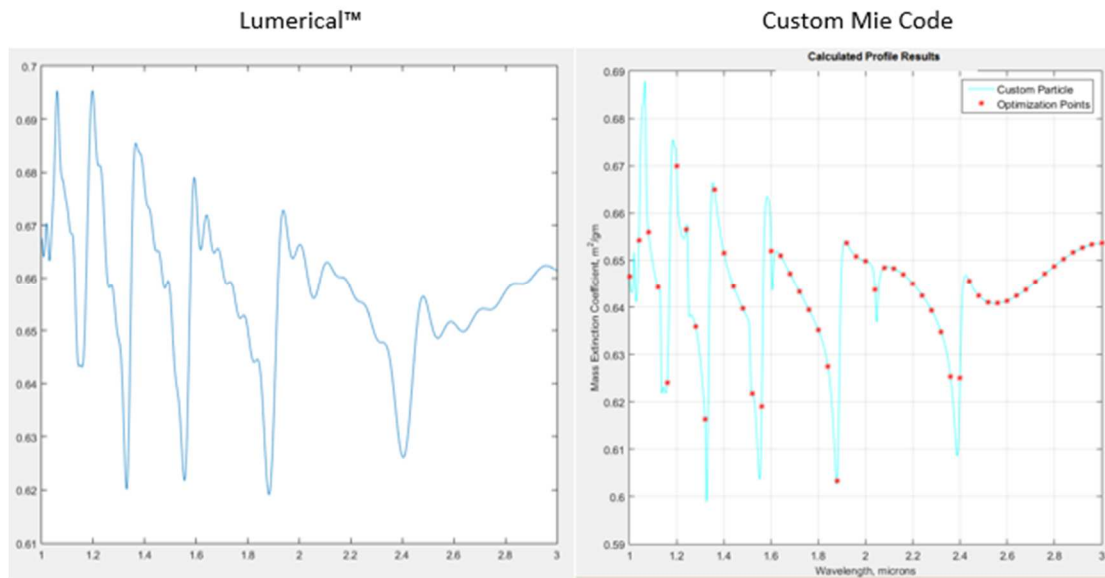


Figure 4-11: Mass Extinction Coefficient results for Lumerical™(left) and custom Mie code (right) for a 2- $\mu\text{m}$   $\text{SiO}_2$  microsphere with 20nm Al shell in the SWIR.

The result of the initial simulation agreed between both programs, proving that both could handle the complex problem and were obtaining similar results despite the different approach. The next two figures display the output from both programs for the MWIR and SWIR filters designed in Section 4.1 and 4.2.

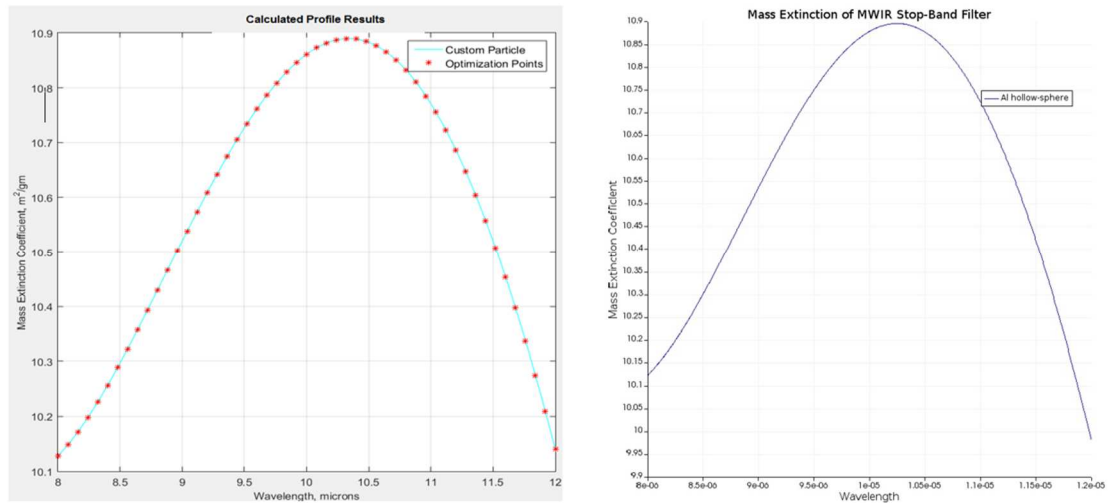


Figure 4-12: Mass Extinction Coefficient results for Lumerical™ (right) and custom Mie code (left) for a 1.95- $\mu\text{m}$  radius 20nm thick Al hollow-sphere in the MWIR.

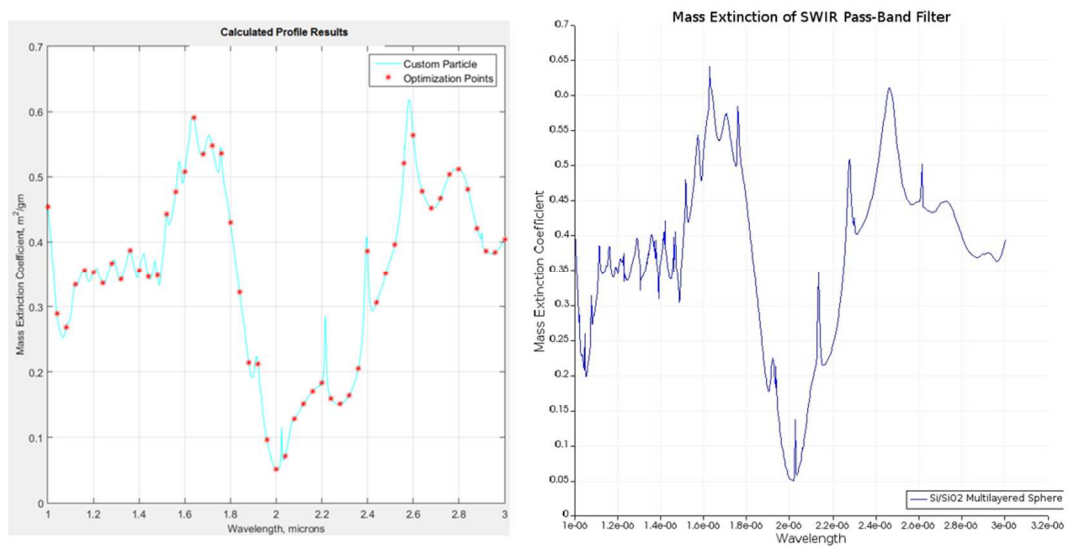


Figure 4-13: Mass Extinction Coefficient results for Lumerical™ (right) and custom Mie code (left) for a multilayered Si/SiO<sub>2</sub> spherical particle in the SWIR.

In these three examples it is clear that our custom Mie solver is able to produce an almost exact match to the Lumerical™ software, successfully validating the findings discussed in this thesis. I was very pleased to see the agreement between the two platforms, because it confirms the precision of the new software, and profoundly improves upon the simulation time needed to evaluate a proposed design. The custom Mie solver takes an average of 10-15 minutes for both optimizations to run their course, while the generation of the scattering coefficients for a single design may take only 1 minute. Conversely, the FDTD software requires a much longer simulation time, depending on particle geometry it could extend upwards of 6 hours.

## Chapter 5

### CONCLUSIONS AND FUTURE WORK

#### 5.1 Conclusions

The research included in this thesis provides a detailed look into the complexities of designing an optical filter through the suspension of constituent micro particles. The custom Mie code developed leverages previously derived recursive algorithms to circumvent the numerical instabilities found in traditional Mie theory when modeling multilayered particles composing of highly absorbing materials. The recursive solver uses ratios of the logarithmic derivatives of the Riccati-Bessel functions to avoid direct calculations of Bessel functions containing large complex arguments. Through the development of this code, two optimization schemes, one driven by the simulated annealing search algorithm, and another by pattern search are used to arrive at an optimal design for multilayered spheres based on user input and design parameters. The code can quickly generate the extinction and scattering profiles of complex multilayered designs to give users insight into the potential viability of an overall optical filter aerosol, as the aerosol's optical properties are heavily dependent on the scattering cross section of an individual particle.

The custom Mie code was used to develop a design for two specific applications, one MWIR broad stop-band filter, and a SWIR narrow pass-band filter. The MWIR stop-band filter utilized an aluminum hollow-shell design where the particle radius and aluminum wall thickness was optimized to generate as high of a mass extinction coefficient over the MWIR band as possible. The SWIR pass-band filter was based upon an alternating high-low index dielectric stack in order to promote interference of incident light inside the sphere. This design used silicon ( $n = 3.44$ ) and silicon dioxide

( $n = 1.43$ ) as the dielectric layered media and a spherical silicon dioxide core. The stack was comprised of three total layers on top of the core and the optimizer was used to determine optimal layer thicknesses in order to attain a window of low extinction centered around the middle of the SWIR band.

Overall, both simulations produced useful designs that accomplished the goal of the specific application. The MWIR reflector was capable of achieving a high mass extinction coefficient approaching  $11 \text{ m}^2/\text{g}$  at its peak, while the SWIR filter was successful in creating an engineered low extinction window in the middle of the band ( $\lambda = 2\mu\text{m}$ ). Both designs and the solutions from the custom Mie code were validated through a comparison with a commercially available 3-D FDTD Maxwell solver known as Lumerical™. The validation proves that a more efficient solver has been created to model multilayered spherical particles and the application of those particles can benefit many different fields including filtering.

## **5.2 Future Work**

The results of this thesis conclude that multilayered spherical particles can be designed to enhance the electromagnetic properties of an aerosol or like suspension, creating highly useful filters. This work can be continued through the fabrication of the proposed particle designs. Work is currently being done to deposit various materials onto microsphere particles through a variety of methods including sputtering, wet chemistry, and chemical vapor depositions, but none of these methods have yet to be perfected. Following the fabrication of these particles, one area of research that could greatly benefit from this research is additive manufacturing [22,23]. Experiments incorporating the multilayered micro particles into existing substrates and composite materials should be performed to test the ability to tailor the Electromagnetic properties

of the structure. If it is found that the concentration of particles can gradually alter the performance of the composite, many new devices and applications can be explored. This thesis provides an encouraging outlook upon the usefulness of engineering micro-particles, however future work will dictate the total impact this research can have on the future of our devices.

## REFERENCES

1. Boxer, C.R., 1968. Fidalgos in the Far East 1550-1770. Oxford University Press.
2. Hunsperger, R.G. and Meyer-Arendt, J.R., 1992. Integrated optics: theory and technology. *Applied Optics*, 31, p.298.
3. Macleod, H.A., 2001. Thin-film optical filters. CRC press.
4. Shi, J., Chen, L., Ling, Y. and Lu, Y., 1998. Infrared extinction of artificial aerosols and the effects of size distributions. *International journal of infrared and millimeter waves*, 19(12), pp.1671-1679.
5. Pratsinis, S.E., 2000. Smoke, Dust and Haze Fundamentals of Aerosol Dynamics. *Journal of Nanoparticle Research*, 2(2), p.209.
6. Klar, T., Perner, M., Grosse, S., Von Plessen, G., Spirkl, W. and Feldmann, J., 1998. Surface-plasmon resonances in single metallic nanoparticles. *Physical Review Letters*, 80(19), p.4249.
7. Balanis, C.A., 2012. *Advanced engineering electromagnetics*. John Wiley & Sons.
8. "The Correct Material for Infrared (IR) Applications." Edmund Optics Worldwide. N.p., n.d. Web. 31 Mar. 2017.
9. Ng, L.N., 2000. Manipulation of particles on optical waveguides (Doctoral dissertation, University of Southampton, Faculty of Engineering and Applied Science).
10. Yang, W., 2003. Improved recursive algorithm for light scattering by a multilayered sphere. *Applied optics*, 42(9), pp.1710-1720.
11. Aden, A.L. and Kerker, M., 1951. Scattering of electromagnetic waves from two concentric spheres. *Journal of Applied Physics*, 22(10), pp.1242-1246.
12. Kerker, M., 2016. *The scattering of light and other electromagnetic radiation*. Elsevier.
13. Bohren, C.F. and Huffman, D.R., 2008. *Absorption and scattering of light by small particles*. John Wiley & Sons.

14. Wiscombe, W.J., 1980. Improved Mie scattering algorithms. *Applied optics*, 19(9), pp.1505-1509.
15. Mackowski, D.W., Altenkirch, R.A. and Menguc, M.P., 1990. Internal absorption cross sections in a stratified sphere. *Applied Optics*, 29(10), pp.1551-1559.
16. Palik, E.D., 1998. *Handbook of optical constants of solids (Vol. 3)*. Academic press.
17. Aarts, E.H. and Korst, J.H., 1988. Simulated annealing. *ISSUES*, 1, p.16.
18. Lewis, Robert Michael, and Virginia Torczon. "Pattern search algorithms for bound constrained minimization." *SIAM Journal on Optimization* 9.4 (1999): 1082-1099.
19. Gerber, H., 1991. Direct measurement of suspended particulate volume concentration and far-infrared extinction coefficient with a laser-diffraction instrument. *Applied optics*, 30(33), pp.4824-4831.
20. Carlon, Hugh R., et al. "Infrared extinction spectra of some common liquid aerosols." *Applied optics* 16.6 (1977): 1598-1605.
21. Gurton, Kristan P., David Ligon, and Rachid Dahmani. "Measured infrared optical cross sections for a variety of chemical and biological aerosol simulants." *Applied optics* 43.23 (2004): 4564-4570.
22. Gibson, I., Rosen, D.W. and Stucker, B., 2010. *Additive manufacturing technologies (Vol. 238)*. New York: Springer.
23. Wong, K.V. and Hernandez, A., 2012. A review of additive manufacturing. *ISRN Mechanical Engineering*, 2012.